ADVANCED HEALTHCARE MATERIALS
www.advhealthmat.de

Biodegradable Piezoelectric Polymers: Recent Advancements in Materials and Applications

*Mohsin Ali, Mohammad Javad Bathaei, Emin Istif, Seyed Nasir Hosseini Karimi, and Levent Beker**

Recent materials, microfabrication, and biotechnology improvements have introduced numerous exciting bioelectronic devices based on piezoelectric materials. There is an intriguing evolution from conventional unrecyclable materials to biodegradable, green, and biocompatible functional materials. As a fundamental electromechanical coupling material in numerous applications, novel piezoelectric materials with a feature of degradability and desired electrical and mechanical properties are being developed for future wearable and implantable bioelectronics. These bioelectronics can be easily integrated with biological systems for applications, including sensing physiological signals, diagnosing medical problems, opening the blood-brain barrier, and stimulating healing or tissue growth. Therefore, the generation of piezoelectricity from natural and synthetic bioresorbable polymers has drawn great attention in the research field. Herein, the significant and recent advancements in biodegradable piezoelectric materials, including natural and synthetic polymers, their principles, advanced applications, and challenges for medical uses, are reviewed thoroughly. The degradation methods of these piezoelectric materials through in vitro and in vivo studies are also investigated. These improvements in biodegradable piezoelectric materials and microsystems could enable new applications in the biomedical field. In the end, potential research opportunities regarding the practical applications are pointed out that might be significant for new materials research.

1. Introduction

Piezoelectricity is the ability to convert applied stress to electric current enabled by a specific material.[1,2] Generally, piezoelectric materials generate charges on two opposite surfaces in response to different mechanical deformation modes such as bending, stretching, and twisting. The unique feature of piezoelectric materials is their non-symmetric crystal structure that allows aligning the opposite ions to form an electric dipole moment. These dipole moments are uniformly oriented in the crystal regions that create domain structures. Upon exposing the material to an external electrical field, the domain orientation will be aligned in a single direction leading to overall uniform polarization of the material and intensifying the piezoelectric response.[3] Once piezoelectric materials are subjected to external stress, the material is polarized along the stress direction, which releases charges in the material, known as direct piezoelectricity.[4]

The application of piezoelectric materials has been investigated in sensation and actuation[5] for developing energy harvesters,[6] electronic skin,[7] smart textiles,[8] and biomedical devices.[9] Representative piezoelectric materials are inorganic ceramics such as lead zirconium titanate (PZT), barium titanate ($BaTiO_3$), potassium sodium niobate (KNN), bismuth-sodium titanate (BNT), and lithium niobate ($LiNbO_3$). However, there are significant concerns regarding the biocompatibility and biosafety of conventional piezoelectric materials that can raise electronic waste (E-waste) or induce

M. Ali, M. J. Bathaei, L. Beker
Department of Biomedical Sciences and Engineering
Koç University
Rumelifeneri Yolu, Sarıyer, Istanbul 34450, Turkey
E-mail: lbeker@ku.edu.tr

E. Istif, L. Beker
Department of Mechanical Engineering
Koç University
Rumelifeneri Yolu, Sarıyer, Istanbul 34450, Turkey

E. Istif
Faculty of Engineering and Natural Sciences
Kadir Has University
Cibali, Istanbul 34083, Turkey

S. N. H. Karimi, L. Beker
Koç University Research Center for Translational Research (KUTTAM)
Rumelifeneri Yolu, Sarıyer, Istanbul 34450, Turkey

The ORCID identification number(s) for the author(s) of this article can be found under https://doi.org/10.1002/adhm.202300318

DOI: 10.1002/adhm.202300318

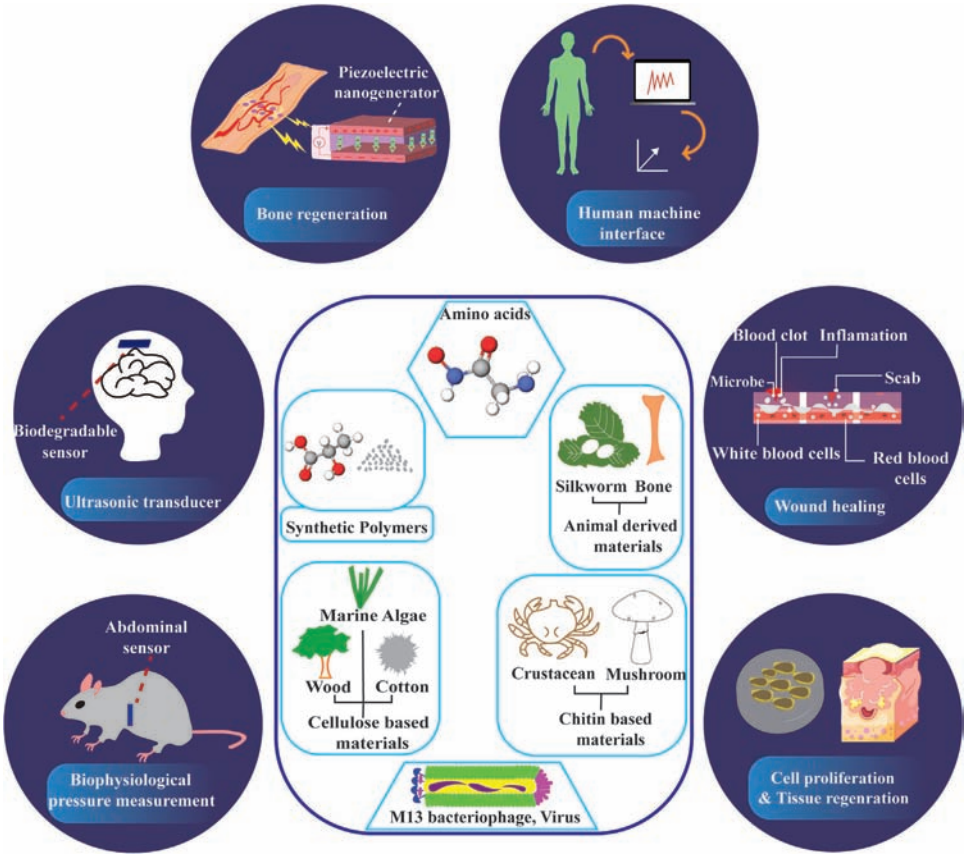

Figure 1. Advancements in biodegradable piezoelectric biomaterials and emerging applications in the medical field, such as bio-physiological pressure measurement (abdominal pressure, intraocular pressure, and intracranial pressure), blood-brain barrier, cell proliferation, human-machine interface, health monitoring, bone regeneration, and wound healing applications.

toxicity in host tissue in the case of implantable medical devices (IMDs). There are two main drawbacks to using lead-based piezoelectrics, such as the brittleness of these ceramics and the toxicity of the lead element.[10] Alternatively, lead-free piezoelectrics have been developed, such as $BaTiO_3$ and KNN; however, the electrical properties of KNN are susceptible to temperature, or BNT has a large hysteresis.[11] Besides, the $BaTiO_3$ has a low Curie temperature, limiting its potential applications.[12] Polyvinylidene fluoride (PVDF) and its copolymers as flexible organic piezoelectrics are some alternatives to ceramic-based inorganic piezoelectrics.[13] However, the major drawback of PVDF is the heart failure (HF) remnants by its degradation, an ultra-toxic acid molecule dangerous to the environment and human life.[14]

In recent years, with the advent of biodegradable piezoelectric materials, there has been an opportunity to alleviate e-waste concerns and improve the biocompatibility of the devices. This category of materials can be utilized to develop implantable medical devices that can perform over a specific timespan in a body environment. Subsequently, they will be absorbed in bodily fluids or degraded to harmless units that eliminate the need for retrieval surgery.[15]

Biodegradable piezoelectric polymers are classified as naturally and synthetically driven polymers. Collagen is one of the natural piezoelectric materials, a soft tissue that mainly contributes to the piezoelectricity of the bone in the human body.[16–18] On the other hand, natural piezoelectric materials can be found in nature. For instance, wood is another raw piezoelectric material due to the presence of cellulose in its structure.[19–21] Poly(l-lactic acid) (PLLA) is one of the synthetically derived biodegradable piezoelectric polymers synthesized by the polymerization of l-lactic acid monomers. The piezoelectric functionality of PLLA is demonstrated as a force sensor in the literature.[22] Even though these biodegradable piezoelectric materials have lower piezoelectricity than ceramic-based ones, several approaches can be applied to enhance their piezoelectricity, such as by modifying their crystal structures.[23–25]

To date, there have been examples of studies regarding the progress in bio-based piezoelectrics and their applications as sensors and actuators.[4,26] However, the available literature needs to thoroughly provide the most recent literature regarding new strategies for developing bioresorbable piezoelectric materials and their utilization for the fabrication of biomedical devices. Thus, this review presents a current and thorough study of biodegradable piezoelectric polymers, emphasizing material structure and their biodegradation mechanisms, followed by their piezoelectricity mechanisms and related applications. Afterward, their most recent and novel applications in physiological sensing, transducers, biomedical devices, and regenerative medicine are comprehensively discussed. The topics are outlined in **Figure 1**, where the review aims to understand the

different categories of biodegradable piezoelectric polymers and their application in fabricating implantable devices for advanced biomedical applications. Finally, we conclude with remarks on future trends, challenges, and opportunities for implementing biodegradable piezoelectric polymers in biomedical applications.

2. Polymers and Structures

First, piezoelectric polymers should have the capability of transformation between mechanical and electrical energy at a specific range to meet the requirements for implementation in biomedical applications. Certain biocompatible and biodegradable piezoelectric materials have been reported that exhibit strong piezoelectric responses. **Table 1** compares the piezoelectric coefficient for biocompatible and biodegradable piezoelectric materials. Although piezoceramic materials show a higher piezoelectric response than natural and synthetic piezoelectric polymers, they contain toxic and non-degradable components, which limit their applications in the fabrication of biomedical implantable devices. On the contrary, different piezoelectric biomolecules, for instance, protein, peptide, and amino acids, are inexpensive and readily available materials. These piezoelectric biomolecules can show great potential in future biomedical applications due to their biocompatibility and biodegradability. Another benefit of using bioresorbable piezoelectric polymers for piezoelectric applications is their low dielectric constant compared with conventional piezo materials.[27–29] Piezoelectric polymers are generally categorized based on their dipole moment and topology. The piezoelectric properties are determined based on the polymer's internal dipole and molecular structure.[30] From their chemical structure, biodegradable piezoelectric polymers can be categorized as i) natural biodegradable piezoelectric polymers and ii) synthetic biodegradable piezoelectric polymers.

Table 1. Comparison of piezoelectric coefficient for different piezoelectric materials.

Bio piezoelectric materials	Type	Piezoelectric coefficient	Ref.
Biocompatible piezoelectric materials			
Aluminum Nitride (AlN)	Ceramic	d_{33} = 3–6 pC N^{-1}	[31]
Barium titanate ($BaTiO_3$)	Ceramic	d_{33} = 190 pC N^{-1}	[32]
Lead zirconate titanate (PZT-5H)	Ceramic	d_{33} = 593 pC N^{-1}	[33]
Zinc oxide (ZnO)	Crystal	d_{33} = 6–13 pC N^{-1}	[34]
Quartz	Single crystal	d_{11} = 2.3 pC N^{-1}	[32]
Polyvinylidene fluoride (PVDF)	Polymer	d_{31} = 23 pC N^{-1}	[34]
Graphene	Single layer	d_{33} = 1.4 nm N^{-1}	[35]
Natural biodegradable piezoelectric polymers			
Diphenylalanine (FF)	Peptide	d_{15} = 80 pC N^{-1}	[36]
Fish swim bladder (FSB)	Protein	d_{33} = 22 pC N^{-1}	[37]
Collagen	Protein	d_{14} = 12 pC N^{-1}	[38]
Cellulose	Polysaccharides	d_{33} = 19.3 ± 2.9 pm.V	[39]
Silk	Protein	d_{14} = 5–1.5 pC N^{-1}	[40]
Lysozyme	Protein	d_{33} = 6.5 pC N^{-1}	[41]
Prestin	Protein	d_{33} = 20 μC N^{-1}	[42]
keratin	Protein	d_{14} = 1.8 pC N^{-1}	[43]
Chitosan	Polysaccharides	d_{33} = 18.4 pC N^{-1}	[44]
Chitin (nanofibers)	Polysaccharides	d_{33} = 9.49 pC N^{-1}	[45]
Cysteine	Amino acid	d_{22} = 11 pC N^{-1}	[46]
Glycine	Amino acid	d_{16} = 178 pC N^{-1}	[46]
Alanine	Amino acid	d_{24} = 17.75 pC N^{-1}	[47]
Proline	Amino acid	d_{25} = 27.75 pC N^{-1}	[48]
Threonine	Amino acid	d_{36} = 6.9 pC N^{-1}	[49]
Leucine	Amino acid	d_{16} = 16.5 pC N^{-1}	[46]
Methionine	Amino acid	d_{34} = 15 pC N^{-1}	[46]
Aspartate	Amino acid	d_{34} = 13 pC N^{-1}	[46]
Histidine	Amino acid	d_{16} = 18 pC N^{-1}	[46]
Synthetic biodegradable piezoelectric polymers			
Poly-γ-benzyl-$_L$-glutamate (PBLG)	Peptide	d_{33} = 25 pC N^{-1}	[50]
Glycine-Polyvinyl alcohol (PVA)	Composite	g_{33} = 5.3 pC N^{-1}	[51]
Polyhydroxybutyrate (PHB)	Polyester	d_{33} = 2.9 pC N^{-1}	[52]
PHB/Zinc oxide	Composite	d_{33} = 13.7 pC N^{-1}	[52]
Poly (D-lactic acid) PDLA	Peptide	d_{14} = 2.28 pC N^{-1}	[53]
Poly (L-lactic acid) PLLA	Peptide	d_{14} = 10 pC N^{-1}	[43]
Poly-γ-methyl-$_L$-glutamate (PMLG)	Peptide	d_{14} = 2 pC N^{-1}	[43]

2.1. Natural Biodegradable Piezoelectric Polymers

Nature can be considered the origin of piezoelectricity. Traces of piezoelectric materials could be found from the living cells and tissues to the jungles and seashores. The piezoelectricity in nature-derived materials was first recognized by using viruses,[54] fish bladders,[37] and prawn shells[55] as piezoelectric generators in electric circuits. Since then, research on organic piezoelectric biodegradable materials has grown considerably. Naturally driven materials possess well-organized structures with low inversion centers and symmetry. Therefore, several biological materials show the inherent ability of linear electromechanical coupling. Since the investigation of piezoelectricity in natural biodegradable materials like collagen,[56] chitin,[57] and cellulose,[56] many bio-based materials have been observed to produce piezoelectricity. Organic biological materials, including small amino acids, proteins, peptides, and polysaccharides with chiral crystal symmetry to the giant hierarchical molecules of biomaterials, featured helical, and fibrous structures with low symmetry.[58] In this section, we will have a comprehensive discussion about these materials.

2.1.1. Proteins and Their derivatives

Amino acids are small monomers that act as building blocks of protein structure. These monomers have different functional groups, such as carboxyl (–COOH), amine ($–NH_2$), and amide. Many studies have reported using protein and its derivatives to fabricate piezoelectric-based devices. Vasilescu et al.[59] conducted the first experiments to find piezoelectric properties in

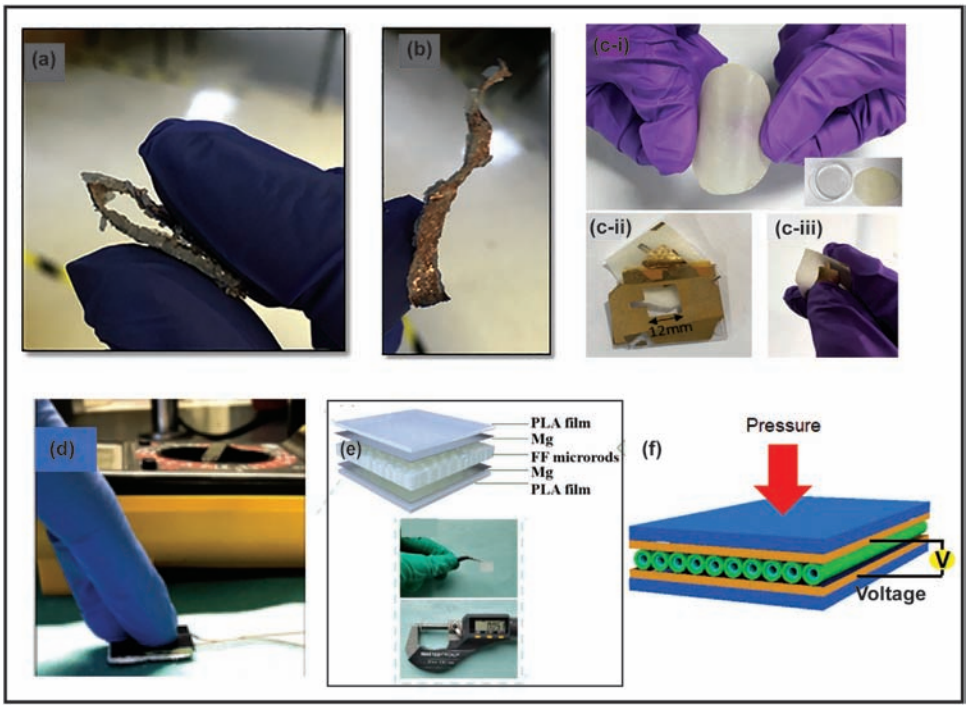

Figure 2. Protein and its derivatives-based devices. a) A completely bent flexible device based on glycine. b) A view of the full-length flexible device with copper electrodes. Reproduced with permission.[64] Copyright 2021, Elsevier. c) i) Chitosan/Glycine film peeled off from petri dish. ii) Gold electrode deposited on both sides. iii) Cs/Gly-based flexible sensor. Reproduced with permission.[65] Copyright 2020, American Chemical Society. d) Generation of the output voltage by manually compressing the DL-Alanine film test. Reproduced with permission.[47] Copyright 2019, American Physical Society. e) Schematic of degradable piezoelectric nanogenerator device based on FF nanorods. Reproduced with permission.[84] Copyright 2021, Elsevier. f) Schematic representation of piezoelectric nanogenerator (PENG) fabricated by utilizing diphenylalanine (FF) nanotubes and porphyrin nanocomposite. Reproduced with permission.[85] Copyright 2022, American Chemical Society.

amino acid crystal structures. In this study, different structures like right-handed (D-Alanine) and left-handed (L-Alanine) "racemic" mixture (DL-Alanine) of D and L amino acid structures were investigated. They discovered the piezoelectric property in many of them except those samples with an anonymous crystal structure. Following the decades, in 2000, Lemanov et al. revealed that the piezoelectricity of amino acids depends on the temperature. Additionally, they reported that the piezoelectricity of γ-glycine and DL-alanine is approaching the value for quartz crystals or even higher.[60–63]

Glycine is the only amino acid with a non-chiral structure. It has three crystal polymorphs known as α-glycine, ß-glycine, and γ-glycine. Okosun et al.[64] studied the repeatable piezoelectric response of films made of glycine/copper under multiple cycles of bending. **Figure 2**a,b depicts glycine/copper film in bending form and an enlarged view of the device displaying copper tape containing an active layer of flexible polycrystalline. Ensieh et al.[65] developed a biodegradable piezoelectric device for measuring pressure based on a chitosan/ß-glycine composite. Figure 2c shows the optical photographs of free-standing CS/Gly film (c-i) and both film (c-ii) and stretchable sensor (c-iii) deposited on a gold electrode. Guerin et al.'s studies and calculations proved that the anti-parallel molecular dipole in the α-glycine crystal structure, which has the space group of $P2_1/C$, leaves no piezoelectricity for this polymorph by canceling net polarization. On the other hand, ß-glycine and γ-glycine have considerable piezoelectric properties. ß-glycine and γ-glycine structures have the space group of $P2_1$ and $P3_1$, which has the piezoelectric coefficient corresponding to d_{22} and d_{33}. Guerin et al. calculated the d_{33} constant for the γ-glycine, and 10.4 pm V^{-1} was reported. The coefficient of shear piezoelectricity, d_{16}, was anticipated to be 195 pm V^{-1} in the ß-glycine phase, which was then verified experimentally through an impedance analyzer and piezometer. Also, they measured the d_{16} coefficient in ß-glycine around 178 pm V^{-1}, which turned out close to the coefficients magnitudes of BTO[66] and KNN.[67] Although amino acids' piezoelectric performances are outstanding, their functionality is not sustainable due to their metastable structure.[68,69]

The ferroelectric phenomenon was also observed in glycine. Several biomaterials exhibit piezoelectric properties, but ferroelectricity is relatively rare. Somewhat differing from this statement, many ferroelectric materials are partly organic. For instance, triglycine sulfate ($(NH_2CH_2COOH)_3$. H_2SO_4) (TGS) is perhaps the most researched.[70] The control of polarization direction upon applying an electric field in biomolecules is known as bio-ferroelectricity.[71,72] It is well-considered that ferroelectricity is in close relation with piezoelectricity. However, the biological importance of bio-ferroelectricity is not poorly assumed. Recently, strong ferroelectricity was found in croconic acid crystal, exhibiting a spontaneous polarization nearly equal to barium

titanate (≈20 μC cm^{-2}) at room temperature.[73] This provoked a new wave of attraction toward low molecular weight organic materials.

Recently, ferroelectricity was observed in the β and γ-form crystals of the glycine, and it is likely to use an external electric field to control the polarization direction.[74,75] The third polymorph of glycine, that is, γ-glycine, is reported as uniaxial, strong piezoelectric,[76] but ferroelectricity and pyroelectricity in this organic compound have not been observed thus far. Heredia et al.[77] stated for the first time that the γ-form of glycine crystal, which shows piezoelectricity, is also a ferroelectric material. Molecular dynamics and density functional theory (DFT) simulations were used to interpret the sources of ferroelectricity in γ-glycine. This study revealed that the small size of glycine molecules results in the realization of very small polarization bits possibly being applicable, i.e., for the storage of ultra-dense information, which is inherently not possible with common ferroelectrics. Bystrov et al.[74] reported the generation of ferroelectricity in β and γ-glycine and found out that β-glycine exhibit better ferroelectric properties compared to γ-glycine. Both forms of glycine crystals have the same molecular volume. However, γ-glycine has shown stronger and more controlled polarization than β -glycine, as it has dipoles in different directions, whereas γ-glycine has spirally oriented dipoles along the axis. These properties of glycine open up an exciting application for bioelectronics logic, sensors, optics, memory devices, and energy generation.

Another amino acid with significant piezoelectricity is DL-alanine, represented by the D and L-alanine racemic mixtures. First, Lemanov et al.[63] confirmed the piezoelectric property of DL-alanine by transmitting high-frequency electrical pulses on a single crystal of DL-Alanine. Subsequently, Guerin et al.[47] utilized density functional theory (DFT) to predict the piezoelectric tensors of DL-alanine. The DL-alanine piezoelectric coefficient was fabricated by drop-casting their crystals on the Cu substrate, and the film was demonstrated as an energy generator through compression. In another study, they have grown racemic amino acid films on copper electrodes to produce energy. The DL-alanine piezo film was manually compressed between electrodes to get the piezoelectricity (Figure 2d). The highest measured value of the longitudinal coefficient (d_{33}) was 4.8 pC N^{-1}. This value was comparable to ZnO and aluminum nitride (AlN) coefficients. Finally, Guerin et al. demonstrated that the DL-alanine piezoelectric crystals could be used as biosensors, energy harvesters, and electronic devices.

Another naturally driven biodegradable piezoelectrics are peptides comprised of amino acid building blocks. Diphenylalanine (FF) is one of the peptides formed by the bond of two alanines-a natural amino acid; it has recently attracted attention due to its outstanding piezoelectricity and mechanical properties in addition to its environment-friendly structure. The FFs are self-assembled structures by hydrogen bonding and π–π stacking, particularly in nanotubes.[36,78,79] In 2010, Kholkin et al. synthesized the FF nanotubes with a strong shear piezoelectric value, measured by piezoelectric force microscopy (PFM) for the first time.[80] These nanotubes have a hexagonal crystal structure (P_6) that contributes to its magnificent shear piezoelectric response (d_{15}) alongside the tube axis. In another study by Vasiliev et al.,[36] d_{33}, d_{31}, d_{14}, and d_{15} coefficients of FF microtubes were measured based on their crystal structure. FF micro-ribbons were fabricated with an orthorhombic shape utilizing inkjet printing and ethylene glycol as solvent by Safaryan et al.[81] It was reported that the coefficient of piezoelectricity d_{15} for orthorhombic FF was around 40 pm V^{-1} by piezo force microscopy (PFM), which was greater than the typically used PVDF polymer. To confirm piezoelectricity in longitudinal mode, a sweep of AC voltage from 0 to 5 V was applied through the tip of PFM placed on a hexagonal peptide nanotube (PNT). A voltage amplitude and displacement slope attributed to d_{33} were calculated at around 18 pm V^{-1}.[36] Other studies reported the d_{33} coefficient of piezoelectricity for FF nanotubes between 9.9 and 17.9 pm V^{-1}.[78,82,83] The measured coefficients stronger response compared to conventional piezoelectric materials. Tao et al.[84] reported a bioresorbable piezoelectric nanogenerator (PENG) by embedding diphenylalanine micro rods into the free-standing film of polylactic acid (PLA) (Figure 2e). The fabricated PENG generated a power output of 1.56 W m^{-3} and an output voltage of 1.76 V. In addition, the device was fully dissolved in phosphate-buffer saline solution, acidic solution, and alkaline solution after 25 days at 60 °C. Kim et al.[85] fabricated piezoelectric nanogenerator device utilizing diphenylalanine (FF) and tetra(p-hydroxyphenyl) porphyrin (THPP) (Figure 2f). The fabricated device exhibited a piezoelectric coefficient of $d_{15} \approx 60$ pm.V^{-1} for FF/THPP nanostructures. The resultant piezoelectric nanogenerators can consistently generate the maximum voltage and current density of 2.6 V and 5.8 μA cm^{-2}, respectively, upon 20 N force exertion. In another study, Park et al.[86] investigated the functionality of diphenylalanine (FF) peptide nanotube-based piezoelectric nanogenerators. The large-scale aligned and unpolarized FF nano-tubes were fabricated using self-assembly methods in different solvent systems. Their optimization results for the alignment of FF nanotubes showed that in ethanol/DI water (75/25) solvent ratio and concentration of 0.4 mg mL^{-1}, the nanotubes exhibited the highest density and uniform alignment at a pulling speed of 20 μm min^{-1}. Regarding the electrical performance of the FF nanotubes-based nanogenerators demonstrated the maximum voltage, current, and power output of 1.66 V, 18.4 nA, and 19.2 nW, respectively, and were stable for more than 3500 cycles.

The orthorhombic form of FF tubes also exhibited ferroelectric-like behavior after the heat treatment. Only half the polarization switching was observed due to the high coercive field when an external electric field was applied.[87–90] Leuchtag et al.[91,92] observed ferroelectric properties with large values of easily switchable polarization and dielectric permittivity[93,94] in branched-chain homopeptide amino acids such as valine (V), Leucine (L), and isoleucine (I).

Natural proteins have unsymmetrical crystal structures. They have the preliminary eligibility for having piezoelectric responses and consist of piezoelectric amino acid blocks. However, their piezoelectric intensity is low in comparison with other materials. Stapleton et al.[41] measured the piezoelectric property of lysozyme. The highest d_{33} coefficient (≈6.5 pm V^{-1}) belonged to tetragonal aggregated films of lysozymes.

2.1.2. Polysaccharide

Cellulose is one of the most common varieties of biopolymers. It is a linear polysaccharide, including glucose as the repeated unit,

and its intrinsic crystalline structure enables piezoelectrical properties. Plant-based biomass (cellulosic) is the most abundant organic, recyclable raw material available on earth and is universally reproduced by nature via a photosynthetic chemical reaction.[95] Cellulose, a major component of wood, lignocellulosic materials, and agriculture biomass residue, has also been investigated for its piezoelectric properties.[96,97] The small wood piezoelectricity in cellulose was an initial idea to study its piezoelectricity resource.[20] The piezoelectricity accounts for hydrogen bonding between the polysaccharide chains in the cellulosic materials.[98] The widely used cellulosic materials demonstrated to show piezoelectricity are cellulose nanocrystals (CNC), cellulose nanofibers (CNF), and bacterial nano cellulosic obtained from onion skin and bleached birch cellulose.[99–102] This variety of cellulose has two polymorphs, triclinic I_α and monoclinic $I_{ß,}$ and both show piezoelectric responses due to the non-symmetric structure of their crystals.[103] However, the piezoelectricity in longitudinal and shear orientation is <1 pc N^{-1}.[104]

Rich cellulosic fibers in citrus fruit's wastes (biomass), along with essential oils, flavonoids, and proteins, present piezoelectric properties. Incorporating orange peel powder into the host matrix of PVDF (up to 40 wt%) resulted in the enhancement of piezo phases (by 70%).[105] The piezoelectric nanogenerator (PENG) developed utilizing orange peel-added PVDF paper offered a power density of 135 μW cm^{-2} and an output voltage of 90 V in response to human motions. Maiti et al.[106] fabricated a piezoelectric nanogenerator device based on onion skin (OS) as piezoelectric material. An OS piezoelectric nanogenerator device is illustrated in **Figure 3**a. Optical photographs of OS show good flexibility of onion skin in bending, rolling, and twisting modes. A study by Sun et al.[19] reported a low-cost, biodegradable wood sponge-based piezoelectric nanogenerator fabricated through a simple delignification process. The maximum voltage and current outputs were 0.69 V and 7.1 nA, respectively, upon applying a 13 kPa pressure level. The mechanical performance of the sponge wood demonstrated excellent compressibility, improving the piezoelectric properties up to 85 times compared to native timber. In a study about 2D $I_ß$ polymorph, Garcia et al.[98] demonstrated that hydrogen bonding is highly responsible for cellulose piezoelectricity due to its asymmetry and polarization between and within chains. To improve the piezoelectricity of cellulose nanocrystal (CNC) films, Miao et al.[107] prepared hydrolyzed CNCs with acid to generate hydrogen bonds on their surface. These surface-modified CNCs composited with Polyethylene oxide (PEO) showed the maximum piezoelectric response of 23 pC N^{-1} (Figure 3b). Cellulose nanofibers (CNF) were also observed, showing ferroelectricity. CNF exhibits small remanence polarization generation upon applying an electric field above ≈40 V $μm^{-1}$. Rajala et al.[108] reported that CNF films require high voltage application (≈40 V $μm^{-1}$) to show ferroelectric characteristics.[109]

Chitin is another category of polysaccharide, one of the components of crustaceans' mushroom cell walls and exoskeletons. It is the second most abundant polysaccharide in the world. It has two distinct polymorphs, α and ß Chitin.[110] In the early 1970s, Fukada et al.[57] found the shear piezoelectricity in the α-chitin. In a recent study, Kim et al.[111] fabricated a biodegradable piezoelectric film made of chitin nanofibers showing good performance and functionality as a flexible piezoelectric device (Figure 3c**)**. The piezoelectricity coefficient of the ß-Chitin nanofibrous film was measured at 4 pm V^{-1}, which agrees with their DFT calculations. Hoque et al.[45] utilized biowaste obtained from crab shells to extract chitin nanofibers. The chitin nanofibers fabricated a thin film piezoelectric nanogenerator with an excellent piezoelectric response. The piezoelectric nanogenerator generated an output voltage of 22 V and short circuit current (I_{sc}) = 0.12 μA.

Chitosan is also a natural polysaccharide that can be extracted from chitin deacetylation. This linear polysaccharide is composed of β-1,4-D-glucosamine.[112] Chitosan has an orthorhombic structure with a nonsymmetric space group of $P2_12_12_{1,}$ and thus it shows the piezoelectric property.[113] Owing to its straightforward water-based solution processing, biodegradability, biocompatibility, low cost, and availability of renewable raw material sources, it is being used in numerous applications.[114–117] A recent study reported the generation of piezoelectricity using chitosan extracted from fungal biomass. Chitosan derived from the fungal biomass showed great potential for utilizing an ecological source of chitosan to fabricate piezoelectric thin films of chitosan.[118] Chitosan has drawn significant attention in research areas including biodegradable sensors and energy harvesters. Such applications are based on the effect of piezoelectricity generated by these materials, which means they can develop electrical charges under mechanical stress.[119] In the preliminary study, the piezoelectric sensitivity of chitosan has been reported[120] as well as in the current study, a vibration sensor based on piezoelectricity of chitosan was developed.[44] The maximum d_{33} coefficient of chitosan reported in this study was 18.4 pC N^{-1}.[44]

2.1.3. Animal-Derived Piezoelectrics

The most common biodegradable piezoelectric polymer in the animal and human body is collagen. This has a ubiquitous presence inside the organs and tissues.[121] In addition to the bone tissue, other collagen-contained tissues like cartilage, ligament hair, and skin can exhibit piezoelectric properties.[7,122–124] Although there is no proven theory about the piezoelectricity mechanism in collagen, a standard theory suggests that piezoelectricity in each polypeptide chain of the collagen is related to the charge dipole corresponding to the amine (N)-carboxyl (C) bound of two ends of amino acids in the one collagen molecule.[18,125] Ghosh et al.[126] fabricated an energy harvesting device utilizing fish skin (collagen) as biodegradable piezoelectric materials. Figure 3d depicts the fabrication method of a fish skin (biomass) based nanogenerator. The developed flexible device acted as a sensor for monitoring physiological signals such as radial artery pulse rate and joint motion (Figure 3e). Vivekananthan et al.[127] developed a piezoelectric nanogenerator device having dimensions 3 cm × 3 cm by utilizing active layers of collagen (Figure 3f).

Some studies have been conducted to reveal the piezoelectric coefficient of collagen recently. For instance, Denning et al.[38] they measured the d_{14} = 12 pm V^{-14} in the fibrillary rat tail collagen via PFM, showing the highest piezo response from the neat collagen. In another study, Zhou et al.[128] studied the molecular mechanism of collagen piezoelectricity based on the twisted collagen model. Their experiments and calculations contributed to understanding the origin of polarization from polar and charged groups in the molecule. In addition, the mechanical stress can change and reorient the dipoles and hence,

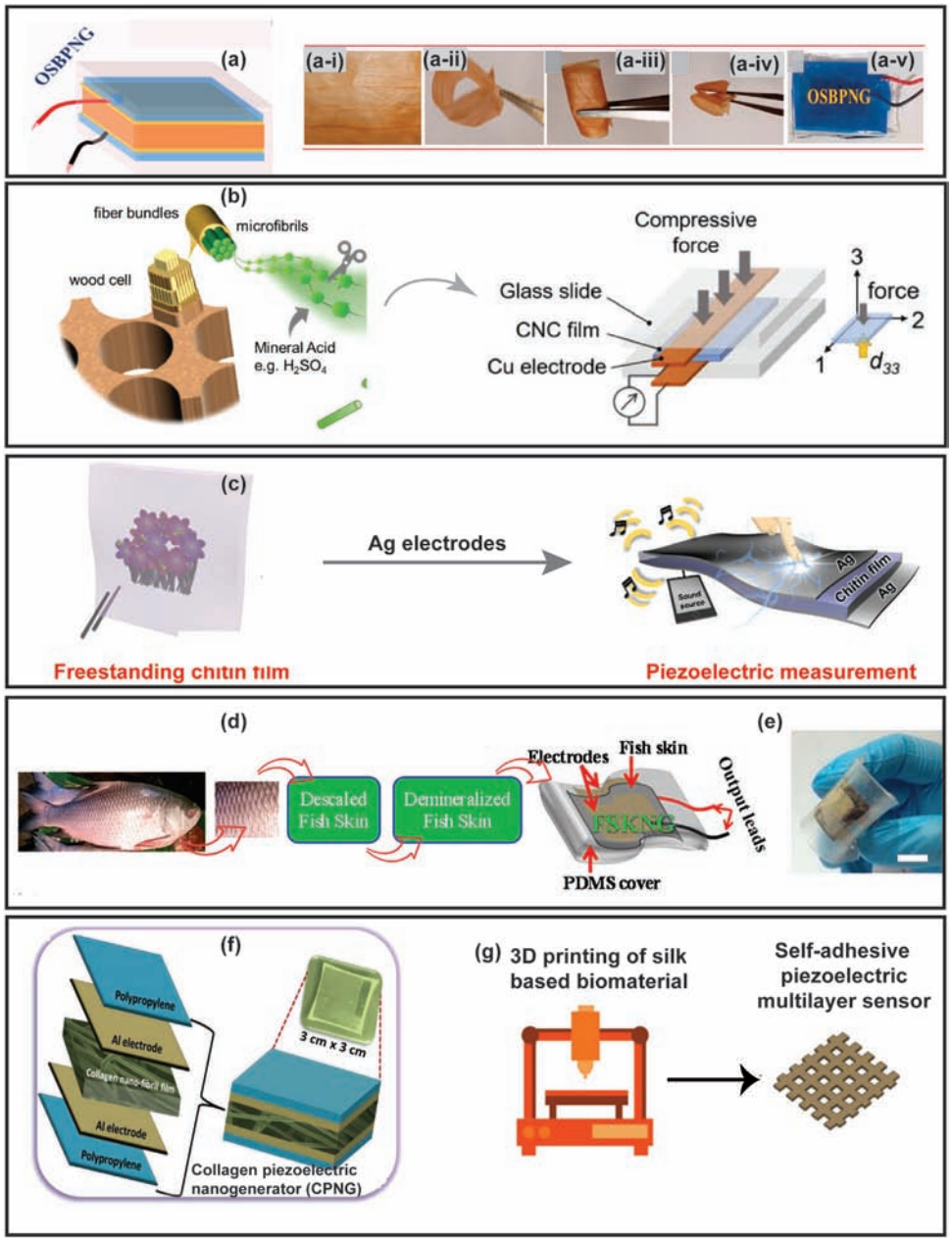

Figure 3. a) i) Cross section view of onion skin bio piezoelectric nanogenerator, ii) film of onion skin, iii) bending of onion skin, iv) rolling of onion skin, and v) twisting of onion skin. Reproduced with permission.[106] Copyright 2017, Elsevier. b) Cellulose nanocrystals derived from wood via sulfuric acid (H_2SO_4) hydrolysis. Schematic of cellulose nanocrystal-based sensor for the measurement of d_{33} (right). Reproduced with permission.[107] Copyright 2021, Elsevier. c) Piezoelectric transducer device based on chitin (piezoelectric material). Reproduced with permission.[111] Copyright 2018, Elsevier. d) Demonstration of the fabrication process of a nanogenerator based on fish skin. e) Optical image of fish skin-based nanogenerator depicting flexibility. Reproduced with permission.[126] Copyright 2017, American Chemical Society. f) Schematic representation of collagen piezoelectric nanogenerator. Reproduced with permission.[127] Copyright 2018, American Chemical Society. g) Multilayer piezoelectric sensor fabricated by 3D printing of silk. Reproduced with permission.[134] Copyright 2022, American Chemical Society.

the magnitude of piezoelectricity. Methods and processes can be applied to create high piezo-responsive systems to enhance the collagen structure's piezoelectricity. Nair et al.[129] made the collagen bundles with self-assembly and by cross-linking them utilizing three crosslinking agents, EDC-NHS (A solution based on 1-ethyl-3-(3-dimethyl aminopropyl) carbodiimide hydrochloride and *N*-hydroxysuccinimide), genipin, and tissue transglutaminase. These three agents enhanced the vertical piezoelectric response of collagen bundles. In another recent work by Bera et al.,[130] they assembled collagen-mimicked tripeptide structures from short peptide sequences. The resulting peptide chain has a helical structure like collagen, and its d_{35} coefficient reached 27 pm V^{-1} thanks to introducing the hydroxyl group.

Silk, an animal-derived material, could be obtained as silk fibroins (SF) from Bombyx mori cocoons or spider silk (SS) from spiders. The silk gains its piezoelectric response from the α-helix and ß-sheet substructures inside its structure.[131,132] Yucel et al.[133] prepared the SF films via a solution drying and consequent draw method. They found that the piezoelectric property of SFs is obtained from ß-sheet generation and uniaxial molecular direction. The shear piezoelectricity property was enhanced by increasing ß-sheet content and crystallinity. The ß-sheet increase resulted from zone drawing of SF films. Therefore, mechanical treatment would be considered a way to increase piezoelectricity in silk. Chiesa et al.[134] introduced biodegradable piezoelectric with soft and holey structures based on 3D-printable silk material for monitoring soft tissues in vivo (Figure 3g). Furthermore, Pan et al.[135] designed a repolarization process for improving the piezoelectricity in the silk fibers. They increase the piezoelectric response of SS fibers from 13.4 to 40.7 mV, thanks to the rearrangement of fibers more orderly manner. Silk was also observed to exhibit ferroelectric behavior. Sencadas et al.[136] reported with the help of PFM results that electrospun and methyl alcohol-treated silk samples show the features of ferroelectric materials. In addition, when electrospun silk fibers were submitted to methyl alcohol vapor, the polymer chains started aligning more oriented fashion, resulting in better ferroelectric response upon high voltage application.

2.1.4. Virus

The M13 phage virus is one of the fascinating biomaterials to mimic biological structures and shows piezoelectric properties. With their filamentous structure clad with helical proteins, these viruses represent a system like human collagen and can mimic its physical properties like piezoelectricity. Due to their phase-changing conformation, highly-ordered crystalline structures can be prepared from the M13 phages.[137] Lee et al.,[54] was the first group to study the piezoelectricity of M13 phages and the piezoelectric coefficient of M13 phages thin film was measured up to 7.8 pm V^{-1} via PFM. They also showed the capability of tuning the phages' piezoelectric response by engineering the coat proteins of filaments. Heo et al.[138] recently fabricated the morphology-modulated hierarchical structures of M13 phage films. Due to the long-range ordered chiral structures from single phage to the macro-scale band of M13s, the piezoelectrical property of M13 phages was enhanced while used as a power generator in a circuit. In another study, Shin et al.[139] improved the piezoelectrical response of M13 by aligning them vertically. They extruded the phages at various speeds into an anodic aluminum oxide template (AAO) until phages filled it with a porous structure. These vertical phage nanopillars yield a d_{33} coefficient of around 10 pm V^{-1}, proving their versatility in several electronic and bioelectronic applications.

2.2. Synthetic Biodegradable Piezoelectric Polymers

Besides naturally driven piezoelectric polymers, another class of biodegradable piezoelectric polymers is synthetically developed piezoelectric materials. Polylactic acid (PLA) and poly-L-lactic acid (PLLA) are two main synthetic biodegradable piezoelectric polymers that will be discussed in the next section, in addition to the other novel synthesized piezoelectric biopolymers.

The PLA has unique piezoelectric properties as a replacement for the common inorganic and organic piezoelectric material.[140,141] PLLA is another conformation of PLA containing L-stereoisomers. The piezoelectricity properties in both PLA and PLLA depend on crystallinity and molecular orientation. These polymers have a semi-crystalline structure with a natural chiral conformation that grants piezoelectricity. The electric dipoles of C=O bonds with an aligned form and branched out of polymer backbone are responsible for piezoelectricity.[142,143] The experiments revealed that the PLLA has piezoelectricity parallel to the z-axis with a d_{14} coefficient of 7–12 pC N^{-1}.[144,145] The stretching treatment in PLA and PLLA can orient the chains and enhance piezoelectricity. Smith et al.[146] measured the piezoelectric coefficient in the highly oriented nanowires grown in the anodized aluminum oxide (AAO) confined environment. The crystallinity of PLLA nanowires was improved by 70% with the nano-confinement method. In the measurements with the PFM, strong shear piezoelectricity was deflected from lateral signals along the nanowires. This deflection yields the value of d_{14} around 8 pC N^{-1}. Curry et al.[22] fabricated a fully biodegradable piezoelectric sensor made by sandwiching the films of piezoelectric PLLA between molybdenum electrodes (**Figure 4**a). They studied the drawing effect on the piezoelectric properties of PLLA. The as-synthesized PLLA film shows three faces of (1 1 1), (2 0 0), and (1 1 0). As the drawing ratio increased, the (1 1 1) plane peak decreased in the PLLA X-ray diffraction (XRD) graph. This is reasoned by the transformation of the α phase of PLLA with the 10_3 helical conformations to the ß phase with the 3_1 helical conformations. The best piezoelectric property was obtained by the drawing ratio of around 2.5 to 4.5. According to this study, it was concluded that the C=O dipoles could align uniaxially by drawing, hence effectively improving the piezoelectricity of PLLA. The alignment of PLLA could also be achieved with the help of electrospinning of aligned nanofibers, resulting in macro piezoelectricity. For instance, Zhu et al.[147] fabricated PLLA porous nanofibrous scaffolds with aligned morphology via melt drawing. They realized the piezoelectricity property in the nanofibers with the size 100 nm and 40 µm. Furthermore, the increase of piezoelectricity was observed with the increase of uniaxial force upon the nanofibers. In another inceptive study, Curry et al.[148] demonstrated a biodegradable device that worked as a force sensor for measuring physiological pressure and an ultrasonic transducer to assist drug delivery and blood-brain barrier opening. The biodegradable device was made of nanofibers of piezoelectric PLLA, PLA encapsulation, and molybdenum electrodes (Figure 4b). Wu et al.[149] fabricated an ultrasonic-driven biodegradable piezoelectric nanogenerator for sustainable electrical signal transmission. This device consisted of fully biodegradable piezoelectric poly(3-hydroxybutyrate-*co*-3-hydroxyvalerate) (PHBV)/Poly (lactic acid) (PLLA)/potassium sodium niobate (KNN) as functional layer (Figure 4c). The voltage and current output levels were increased to 6 V, and 0.5 µA, respectively, by a 50% increase in KNN amount. Yousry et al.[150] developed a conformable shear mode ultrasonic transducer based on bioresorbable piezoelectric PLLA nanofibers. A wide range of frequency (500 kHz) was applied to evaluate the electromechan-

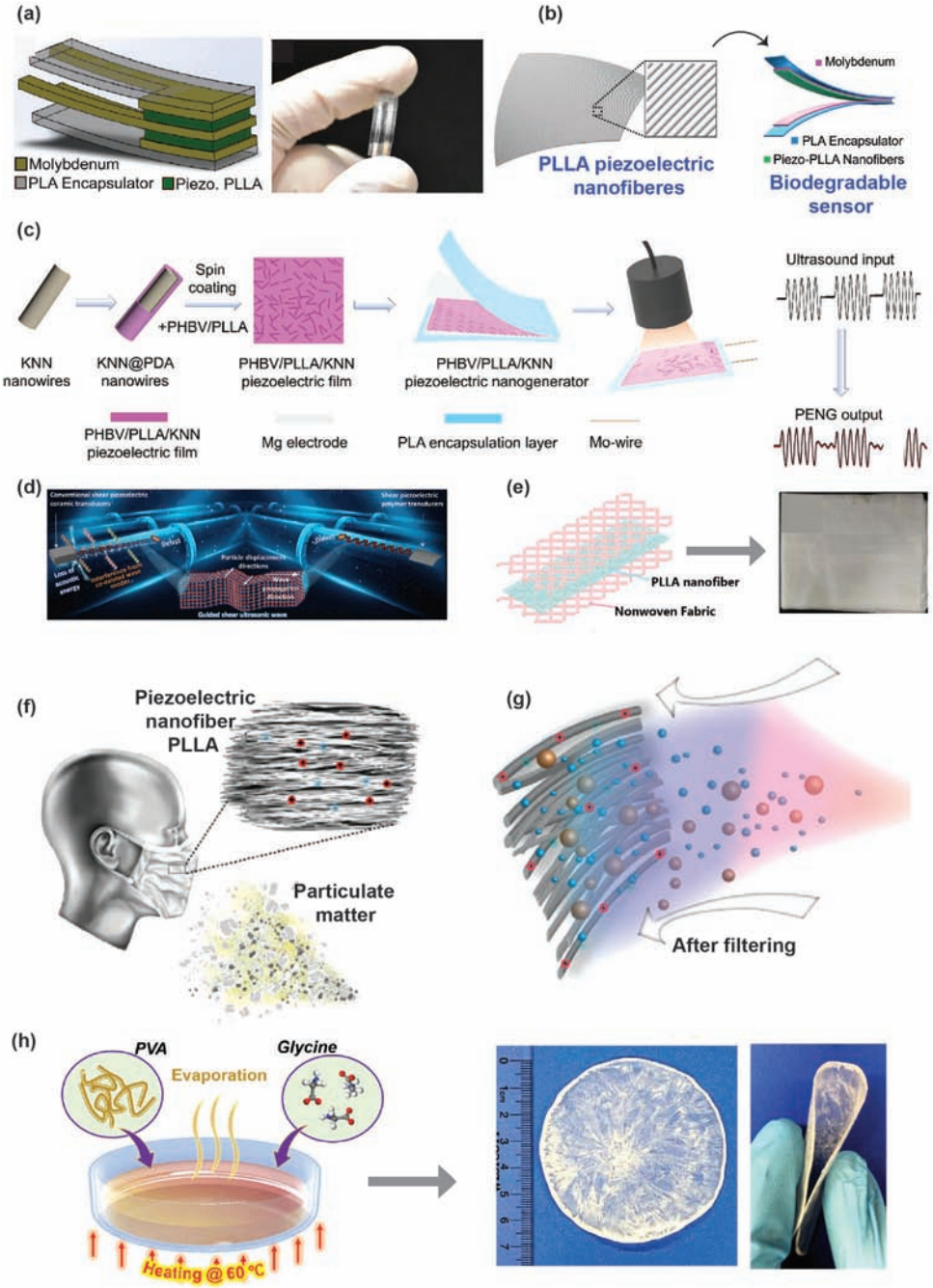

Figure 4. Bio-decomposable force sensor based on piezoelectric PLLA. a) A simple illustration of the piezoelectric and biodegradable sensor (left) and optical photograph of the developed piezoelectric and bio-decomposable sensor (200um thick and 5 mm × 5 mm) (right). Reproduced with permission.[22] Copyright 2018, Proceedings of National Academy of Science. b) A simple representation of processed piezoelectric PLLA nanofibers (left) and schematic illustration of the biodegradable pressure sensor (right). Reproduced with permission.[148] Copyright 2020, Proceedings of National Academy of Science. c) Representation of fabrication process of PHBV/PLLA/KNN composite film-based nanogenerator. Reused with permission.[149] Copyright 2022, Elsevier. d) A schematic representation of underwater structural health monitoring technology by guided ultrasonic waves utilizing a shear piezoelectric polymer-based transducer compared to a shear piezoelectric ceramic transducer. Reused with permission.[150] Copyright 2023, Wiley-VCH GmbH. e) Schematic demonstration of PLLA filter structure (left) and optical image of PLLA filter membrane (right). Reproduced with permission.[53] Copyright 2019, Wiley-VCH GmbH. f) Concept photograph and schematic illustration of facemask using electrospun biodegradable piezoelectric PLLA nanofibers. g) The combined influence of mechanical sieving and increased electrostatic adsorption is because of the piezoelectric effect in trapping particles. Reproduced with permission.[151] Copyright 2022, Wiley-VCH GmbH. h) Schematic representation of the synthesis of PVA-glycine biodegradable piezoelectric films (left). The Right image is the optical image of a wafer-sized grown flexible film. Reproduced with permission.[51] Copyright 2021, American Association for the Advancement of Science (AAAS).

ical responses over the macroscopic area of the transducer. The fabricated biodegradable ultrasonic transducer showed a high level of sensitivity in detecting imperfections in air and liquid. Further, the developed PLLA does not require electric poling to impart piezoelectricity because the shear mode originates from the chemical structure of PLLA itself. The shear mode ultrasonic transducer based on PLLA shows great potential for underwater structural health monitoring applications. Figure 4d schematically presents the underwater structural health monitoring technique with the help of ultrasonic shear waves utilizing shear piezoelectric ceramic-based transducers compared with transducers based on shear biodegradable piezoelectric polymers. The shear mode piezoelectric polymer-based transducers contain in-plane mechanical coupling, not needing electrical poling, are low profile, and shapes conformal; shear ceramic piezoelectrics are not shaped conformal, needed electrical poling, and have a high profile. Zhang et al.[53] demonstrated electrospun-based PDLA/PLLA nanofibers (Figure 4e, left) that improve filtration efficiencies for removing small particulate matter (PM). The surface charges generated from piezoelectric PLLA membrane (Figure 4e, right) with controllable porosity demonstrated great improvement in capturing small-sized particles (i.e., PM2.5). Additionally, they demonstrated the fabrication optimization parameters, such as solution concentration and electrospinning time to improve the quality factor, up to 4.6% compared to conventional 3 M respirator filters. Le et al.[151] fabricated a highly efficient, recyclable, self-sustaining, and humidity-resistant air filtration membrane utilizing biodegradable PLLA nanofibers with stable piezoelectricity and long-term biodegradability (Figure 4f). Based on the effect of aeolian vibrations, the self-charged PLLA nanofibers membrane (Figure 4g) permits the joined impact of mechanical sieving, and it increases electrostatic adsorption to eliminate particulate matter (PMs). In the current studies, researchers are developing synthetic biodegradable piezoelectric polymers utilizing natural piezoelectric materials.

For instance, Yang et al.[51] demonstrated a self-assembly-based and wafer-scale approach to fabricate a PVA-glycine-PVA sandwich structure. Figure 4h depicts the synthesis route of the glycine-PVA-based bioresorbable piezoelectric film. The sandwiched piezoelectric structure exhibited an impressive piezoelectric response ($g_{33} = 157.5 \times 10^{-3}$ Vm N^{-1}) comparable to commercial piezoelectric materials such as PVDF-TrFE. The sandwiched piezoelectric structure exhibited an impressive piezoelectric response ($g_{33} = 157.5 \times 10^{-3}$ Vm N^{-1}) relative to commercial piezoelectric materials such as PVDF-TrFE.

3. Piezoelectricity Mechanisms in Biodegradable Polymers

Re-orientation of the dipoles of the molecule in the bulk polymer is known as the piezoelectricity phenomenon. Piezoelectricity in organic materials can be attained in different ways, such as by drawing (stretching) or applying an external electric field. In recent years, graphene, self-assembled diphenylalanine peptide nanotubes (PNTs), silk, collagen, and glycine have been studied widely for their piezoelectric properties.

Shear piezoelectricity has also been observed in self-assembled diphenylalanine (FF) peptide nanotubes (PNTs).[80,152] PNTs are amino acids' building blocks and are considered suitable options for developing "green" piezo devices and piezoelectric material. Guerin et al.[49] examined piezoelectricity in polycrystalline films of amino acids. Chiral enantiomers and polarization in the longitudinal direction of alanine amino acids are demonstrated in **Figure 5**a,b, respectively. The same group reported longitudinal piezoelectricity along the 3axis of the L-alanine and DL-alanine crystals (Figure 5c). The piezoelectric shear constant of PNTs was reported at approximately $d_{15} = 60$ pm V^{-1}.[80] The mechanism of piezoelectricity in diphenylalanine nanotubes (FF) is mainly due to the directions and sizes instead of uniform and unidirectional growth; generating piezoelectricity in a macroscopic order is challenging for diphenylalanine (FF) PNTs. The problem originated from the polarization made in the radial direction, while in the axial direction, the polarization is eliminated due to irreversible phase transition. The coercivity in the axial direction allows piezoelectricity in diphenylalanine (FF) PNTs only in the breakdown voltage.[153,154] On the other hand, researchers attempted to control nanostructured FF's growth. For instance, Nguyen et al.[82] grew epitaxial uniform FF micro rods with hexagonally arranged nanochannels for the first time and measured a d_{33} value of 10 pm V^{-1}. Once more,[83] they controlled the polarization of FF microrods by applying an electric field during their self-assembly process. Finally, uniform polarization was obtained at around 18 pm V^{-1} for the d_{33} constant. Therefore, there will be potential for applying nano FFs beyond energy harvesting and biomedical devices if their structure and polarization are precisely controlled.

Glycine is comprised of amino acids, and three different crystalline phases (named α, β, and γ phases) were realized based on the availability of the crystalline region in glycine.[155] Alpha glycine shows non-crystalline nature due to centrosymmetric, resulting in no piezoelectricity.[46] Crystalline γ glycine can show three piezoelectric constants in the longitudinal direction (Figure 5d).[64] Figure 5e depicts the corresponding structures of β and γ glycine crystals with measured piezoelectric coefficients.[156] Shear piezoelectricity was observed in β and γ-glycine owing to the acentric symmetry.[157] The constant of piezoelectric voltage and the constant of a piezoelectric strain of β-glycine was reported around $g_{16} = 8$ Vm N^{-1} and $d_{16} = 190$ pm V^{-1}, respectively.[46] As an organic material, glycine is considered a potentially valuable and suitable candidate for biotechnological and biomedical applications because of its biocompatible nature, controlled biodegradability, and high piezoelectricity.

The piezoelectric phenomenon produced in collagen is due to the charge group and polarity present in the molecule.[128] Dipoles of molecules in these residues reorganize towards the collagen molecule's elongated axis under mechanical force/stress that changes the magnitude of the dipole moment. Simultaneously, piezoelectricity generates collagen due to these effects.[128] Vivekananda et al.[127] utilized collagen nanofibers as a piezoelectric material for developing an energy-harvesting device. The structure of the collagen molecule that offered piezoelectricity because of the presence of amino acids and peptide bonds is demonstrated in Figure 5f. The value of the piezoelectric shear constant of collagen is $d_{14} \approx 0.1$ pm V^{-1},[18] and this value can be enhanced by changing the pH from acidic to neutral or by incorporating chitosan.[158]

Silk material contains combined phases of crystalline and amorphous.[159] The combination of higher crystalline

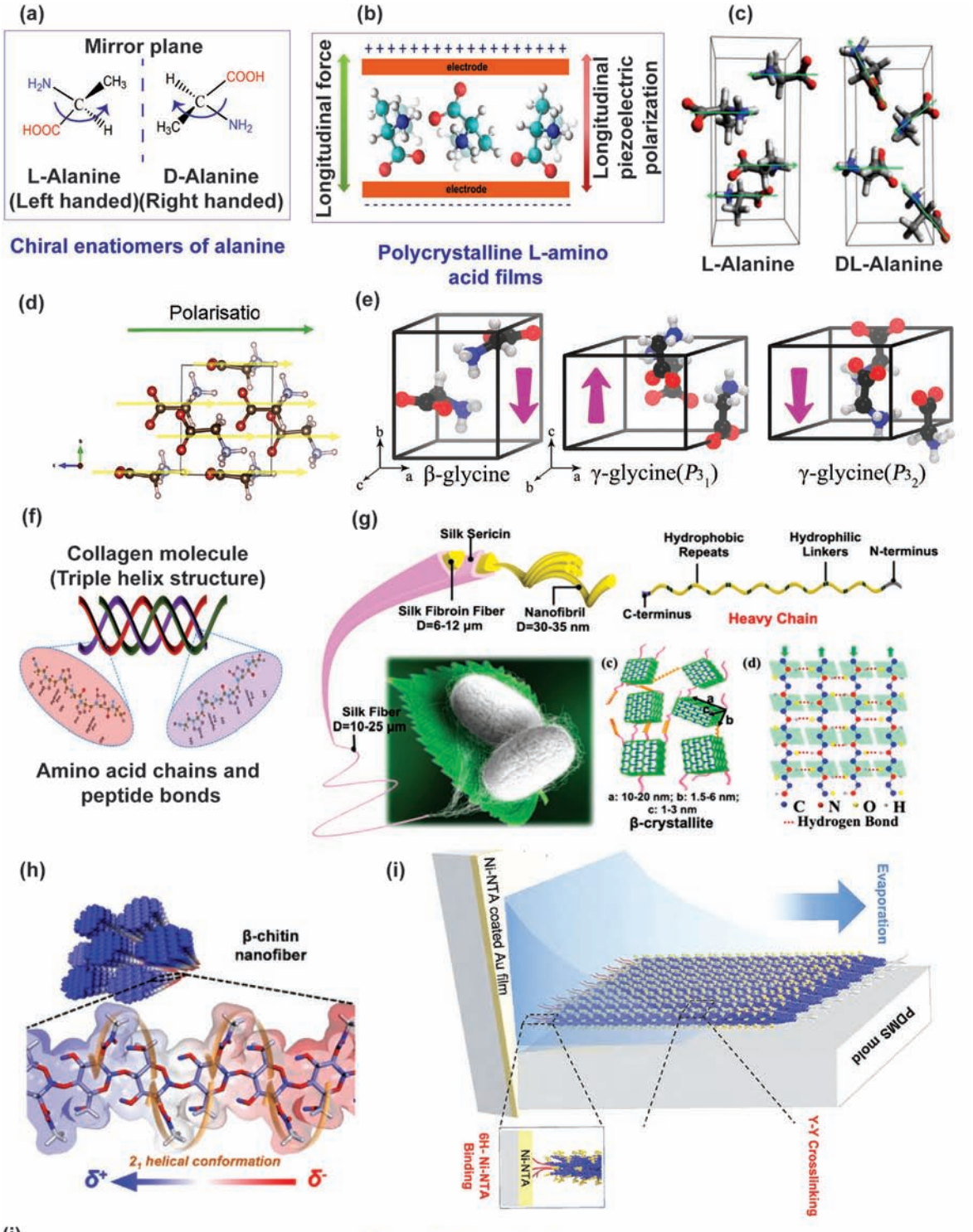

orientation, β-sheet crystallinity, and a high degree of silk II generate piezoelectricity in silk.[133] Figure 5g graphically presents silk's hierarchical, heavy chain, and β-sheet crystalline structure.[160] With a draw ratio of 2.7, silk films show a shear piezoelectric d_{14} constant value around ≈1.5 pC N^{-1}.[133] Silk fibroin is utilized in bone fracture healing,[161] regenerative medicine,[162] and tissue engineering.[163] Fabrication of wearable sensors and microfabricated biomedical devices based on silk is enabled through silk piezoelectricity.

The hierarchical fibrous structure and low symmetry of natural polysaccharide materials like chitin and cellulose exhibit considerable piezoelectricity. Cellulose is one of those materials initially found to show a piezoelectric response.[166–168] Cellulose Crystallites orient themselves in wood over positive and negative orientation according to z-direction while randomly oriented in the x–y plane.[167] Cellulose derived from wood has two polymorphs, I_α and I_β.[169] A triclinic crystal structure with no symmetry was observed in $I_{\alpha,}$ while I_β comprised a monoclinic crystal structure. In the cellulose crystal model, where hydrogen bonding (HB) is responsible for in-plane intermolecular interactions, layers of cellulose crystals are joined by Van der Waals (VdW) forces, and covalent bonding creates interconnections between the chains.[98]

Chitin is comprised of *N*-acetyl-D-glucosamine units by covalent bonding.[117,170] Since chitin and cellulose are similar in structure, chitin was also observed to show piezoelectricity.[170] Chitin is reported in three polymorphs named α, β, and γ. A recent study by Kim et al.[111] explained the difference in piezoelectricity in both α and β-chitin. As depicted in Figure 5h, the overall polarization shown by β-chitin is highly one-directional, with a total theoretical polarization of 1.87 C m^{-2} along the [0 0 1] orientation. At the same time, overall weak polarization was observed for α-chitin along all electric field directions.

M13 phage is a long rod-like virus bacteria with a 6.6 nm diameter and ≈939 nm length. The presence of piezoelectricity in the M13 phage is enabled by chemical and genetic flexibility that shows operational forms and rod-like monodispersed structures with the potential for self-assembling into different hierarchical shapes. The generation of piezoelectricity in the M13 phage is due to the fivefold rotational arrangements of its main coat protein and twofold symmetry (Figure 5i).

The thermodynamically stable α crystalline PLLA contains randomly oriented dipoles of C=O along the main chain. To impart piezoelectricity, randomly oriented chains of molecules must be processed (thermal stretching) to transform the α-crystalline form of PLLA to β crystalline. This conversion of the randomly oriented chains of molecules rearranges the molecular chains in the stretching direction.[165] Figure 5j (right) shows C=O dipoles of the molecule that can also be aligned with the electrospinning process to generate piezoelectricity in PLLA films. Besides piezoelectricity, PLLA is a flexible and translucent polymeric. This material is derived from plants, and due to its environment-friendly nature, it is being utilized in mobile device applications.[171] However, PLLA still has a lower piezoelectric constant value than inorganic materials, for instance, PZT. The stretched films of PLLA do not show spontaneous polarization, unlike PVDF polymer processed by poling, but still provide a significant shear piezoelectric constant.[172] It is possible to control the percentage crystallinity of PLLA as it has an intricate higher-order structure consisting of intermingled amorphous and crystalline regions. Thus, the piezoelectric constant can be engineered by increasing the orientation of molecules and the degree of crystallinity of PLLA film. Because of the biocompatibility and biodegradability of PLLA film, it has offered promising applications in actuators and biodegradable force sensors.[4,148] Recently, a PLLA nanofiber-based air filtration membrane was developed for reusable and humid-resistance face mask application. The working mechanism is based on the charge generation of piezoelectric PLLA strands, preventing the penetration of viruses or bacteria into the facemask. The long-term biodegradability and reusability of the PLLA-based face masks offer an eco-friendly solution to massive plastic waste from conventional non-degradable masks.[151]

4. Biodegradation Mechanism

4.1. Proteins/Peptides/Amino Acids

Water solubility is a property of proteins, peptides, and amino acids. These naturally driven materials can be decomposed into fundamental molecules in an aqueous environment. The residue of proteins, amino acids, and peptides can be reabsorbed or remain in the host system devoid of activating extreme immunogenic responses. Glycine is an essential nutrient that plays a vital role in anti-oxidative reactions, metabolic regulations, and neurological function. According to studies, glycine is produced in several mammals, including biomolecules like threonine, choline, and serine. Glycine enters and is catabolized easily through the small intestine, degrading to form carbon dioxide (CO_2) and ammonia.[173] The time-dependent degradation of a glycine-based pressure sensor in phosphate buffer saline (PBS) solution has been illustrated in **Figure 6**a.[65] The biodegradable

Figure 5. a) Chiral amino acids with longitudinal piezoelectricity. Structure schematic for chiral enantiomers of alanine. The left side shows L-Alanine, and the right side depicts D-Alanine. b) Illustration of longitudinal polarization of amino acids films in polycrystalline phase. Reproduced with permission.[49] Copyright 2018, American Chemical Society. c) The green arrows in the unit cell show the arrangements of alanine's molecular dipoles, which correspond to the orientation and magnitude of piezoelectric responses. Reproduced with permission.[47] Copyright 2019, American Physical Society. d) The crystal structure of γ-glycine shows three longitudinal piezoelectric coefficients. The unit cell shows the green dipole, while the yellow color shows molecular dipoles. Reproduced with permission.[64] Copyright 2021, Elsevier. e) Structure of β and γ glycine along with measured polarization constants. White, blue, red, and black showing hydrogen, nitrogen, oxygen, and carbon, respectively. Reproduced with permission.[156] Copyright 2019, American Chemical Society. f) Molecular chain of tri-peptide nano-fibrils of collagen showing the sequence of different amino acids. Reproduced with permission.[127] Copyright 2018, American Chemical Society. g) Schematic representation of hierarchical (left) and molecular/chemical formation of silk (right). Reproduced with permission.[160] Copyright 2019, American Chemical Society. h) Structure of β-chitin nanofibers showing polarization. Reproduced with permission.[111] Copyright 2018, Elsevier. i) Representation of template-assisted vertically aligned phage of M13 showing piezoelectricity. Reproduced with permission.[164] Copyright 2019, American Chemical Society. j) Structural schematic of PLLA chains showing the orientation of C=O in all directions (left) and desired orientation of dipole of C=O after the process of electrospinning. Reproduced with permission.[165] Copyright 2017, Royal Society of Chemistry.

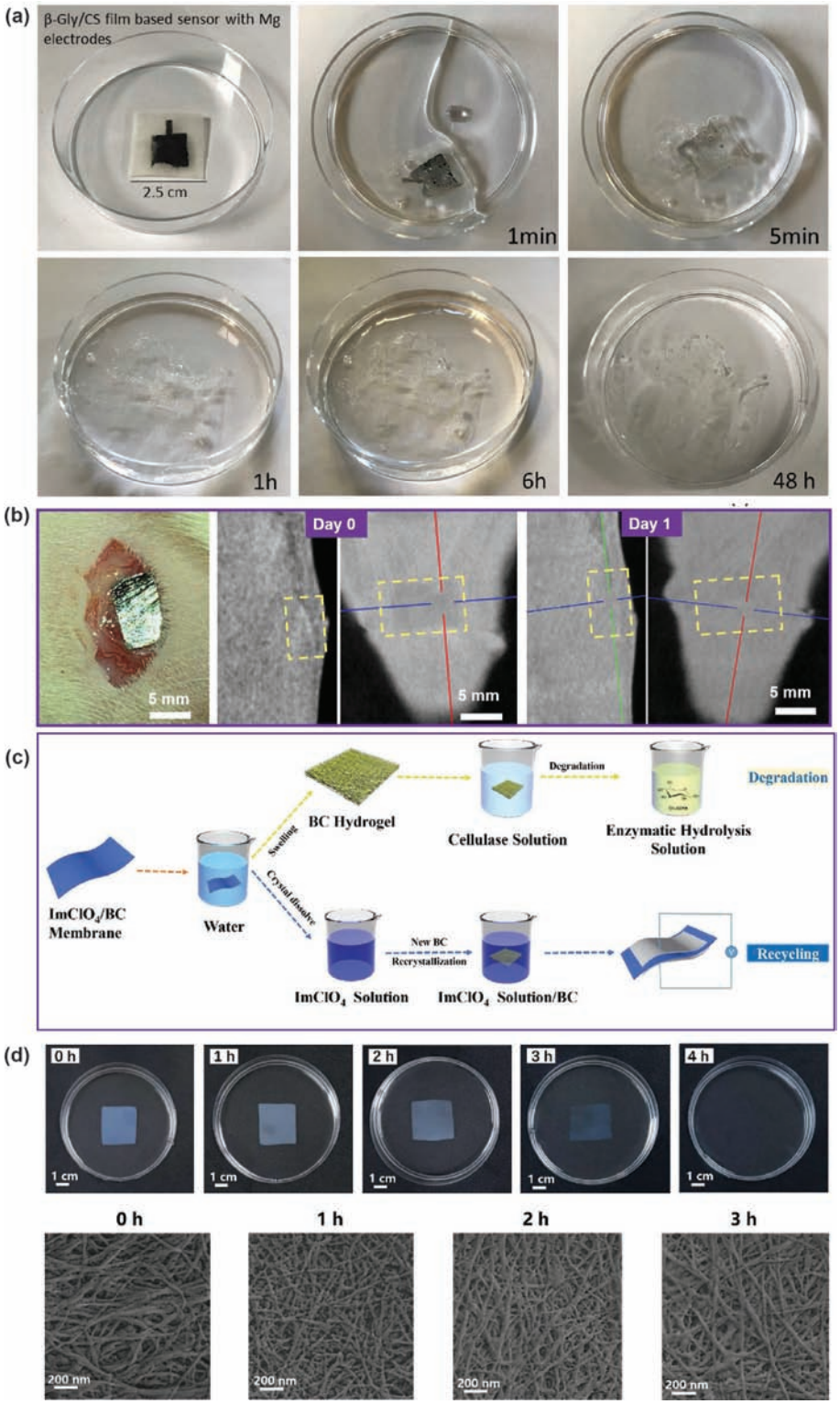

Figure 6. a) Optical photographs depicting the biodegradation of Chitosan/glycine pressure sensor in PBS solution. Reproduced with permission.[65] Copyright 2020, American Chemical Society. b) Examination of biodegradation of bioresorbable piezoelectric glycine-PVA film embedded in a rat body at the subdermal dorsal section. The left optical image depicts the piezoelectric sensor being implanted; the center and right photographs are computed tomography (CT) images of the implanted section immediately and after 1 day of the implantation, respectively. Reproduced with permission.[51] Copyright 2021, AAAS. c) Illustration of a process showing biodegradation and recyclability of the hybrid sensor. d) Optical images demonstrate the decomposition process of the sensor. The sensor membrane is completely decomposed in the cellulose solution (5 mg mL^{-1}, 50 °C) after 4 h. Reproduced with permission.[15] Copyright 2022, American Chemical Society.

piezoelectric sensor based on glycine was dissolved entirely in PBS solution after 48 h of immersion. A study by Yang et al.[51] reported in vivo biodegradation of the sandwiched film after implantation of the PVA-glycine device in the dorsal region of the rat. The device completely disappeared after one day, and no toxic effects were observed in the surrounding tissues (Figure 6b). In mammals, diphenyl alanine peptides participate in the essential alanine-glucose cycle between tissue and the liver. A bacteria in the intestine known as *Escherichia coli* (*E. Coli*) can decompose alanine.[174] In a recent study, Kim et al.[85] reported that the biodegradation assays showed a significant decrease in the peak intensity of FF nanotubes after immersion in PBS for 5 minutes. However, tetra(*p*-hydroxyphenyl) porphyrin (THPP)-incorporated FF nanostructures were slightly degraded after 5 min. Thus, the degradation rate can be tuned by controlling the THPP concentration, as it affects the thickness of the film layer.

4.2. Polysaccharides

Cellulose offers good biocompatibility and can decompose only by fungal and microbial enzymes.[175] The degradation of cellulose inside the body is challenging because of the shortage of hydrolytic enzymes that strike the linkages.[176] Cellulose can be degraded efficiently by organisms, but they still have to produce a battery of enzymes that activate together to make the degradation happen.[175] In vivo degradation of cellulose has been reported by research studies (for example, reformed cellulose is likely to be decomposed and absorbed over the weeks based on the quantity and location), and natural piezoelectricity might be affected because of the change in chemical structure and crystallinity.[177,178] In vitro degradation of piezoelectric hydrogel membrane based on bacterial cellulose (BC) and imidazolium perchlorate has been demonstrated by Lu et al.[15] Figure 6c depicts the degradation and recyclability of the BC hybrid. Optical images demonstrate that the BC hybrid sensor completely dissolved in cellulase solution after 4 h of immersion (Figure 6d).

Degradation of chitin-based materials is reported through hydrolysis by lysozymes (an enzyme available in mammals).[179–181] In vivo and in vitro decomposition studies of chitin and its deacetylated derivatives were conducted by Tomihata et al.[179] Films of 150 um thickness were prepared with different percentages. For the in vivo study, the back of the Wistar rat (subdermal tissue) was considered, while in vitro study was performed in PBS solution comprising lysozymes. Pure chitin was observed to show quick degradation compared with other derivatives showing 20% and 50% remaining weight after they were inserted in rats for 2 weeks and dipped in PBS solution for 30 h. Kim et al.[111] demonstrated in vitro degradation of piezoelectric chitin film in chitinase solution. **Figure 7**a shows the time-dependent decomposition of 35 μm chitin film in the solution of chitinase at room temperature for 8 days. The percent weight loss of chitin film was reduced over time in the chitinase solution (Figure 7b). By adjusting the concentration of chitinase, the degradation rate can be controlled. The degradation time was decreased to ≈4 days with 5 UN chitinase/10 mL of concentration (Figure 7c). Generally, polysaccharides have biocompatible and biodegradable nature as a significant advantage. Although there were intermittent studies regarding their piezoelectricity, efficient techniques are needed to improve the piezoelectric coefficient.

4.3. Silk and Collagen (Animal Derived Polymers)

Polymers based on collagen and silk are enzymatically decomposable, which demands catalysis for effective decomposition under a physiological environment. For example, carboxylase, actinase, and chymotrypsin can impart good degradation to silk polymers.[182–184] It was found through in vitro study that the amorphous part of the silk can be degraded immediately over the initial days in an enzymatic solution,[185] but the highly oriented part (crystalline phase) requires prolonged time (15 days) for decomposition.[186] Chiesa et al.[134] demonstrated in vitro degradation of 3d printed silk-based piezoelectric material in PBS solution. Figure 7d illustrates the immersion of silk-based piezoelectric material in PBS solution at body temperature (37 °C). The degradation plot over time demonstrates that most of the samples were completely dissolved in solution in three weeks except those samples containing crystalline parts (Figure 7e). Compared with in vitro decomposition of silk in PBS enzymatic solution, the external reaction mechanism was utilized to decompose silk in vivo, having no immunogenic response. Although, the prolonged time required may be months to years to degrade silk material in vivo. Wang et al.[184] studied different behavior in the degradation of silk scaffolds implanted in Lewis rats and nude mice were observed from different methods. Those findings revealed that biodegradation behavior could be improved by modifying the processing methods and crystallinity.

Collagen shows immediate degradation behavior in vivo compared with silk-based materials. Radiolabeled proline was found as an essential element in collagen, showing the decomposition rate of skin collagen in adult rats between 3% and 5% per day.[187] Alberti et al. analyzed the bio decomposition of highly oriented collagen fibrils in Sprague-Dawley rats.[188] They observed that vulcanizing collagen with glutaraldehyde could increase stability. Although non-vulcanized collagen scaffolds were immediately decomposed by detecting no fiber morphology after 21 days, the crosslinked samples were intact under the same condition for 3 weeks. Animal-derived polymers are considered an active candidate for bioelectronics despite their low piezoelectric coefficient compared with commercially used piezoelectric materials because of their low immune response, good biocompatibility, and controlled degradation.

4.4. Virus

Celec et al.[189] initially studied the in vitro biodegradation of M13 phage for different body tissues and fluids. Other fluids and tissues present in the body were used in vitro, involving the colon, jejunum, urine, saliva, blood, and stomach homogenates for examining M13 phage survival. The fast complete biodegradation of M13 phage was noticed in jejunum after 45 min owing to the presence of proteolytic enzymes in the homogenate. M13 phage was decomposed almost 88%, 66%, and 44% after 45 min in salvia, urine, and blood, respectively. Even though the virus exhibits good piezoelectricity, the phage film's piezoelectric response was not completely understood. An in-depth investigation

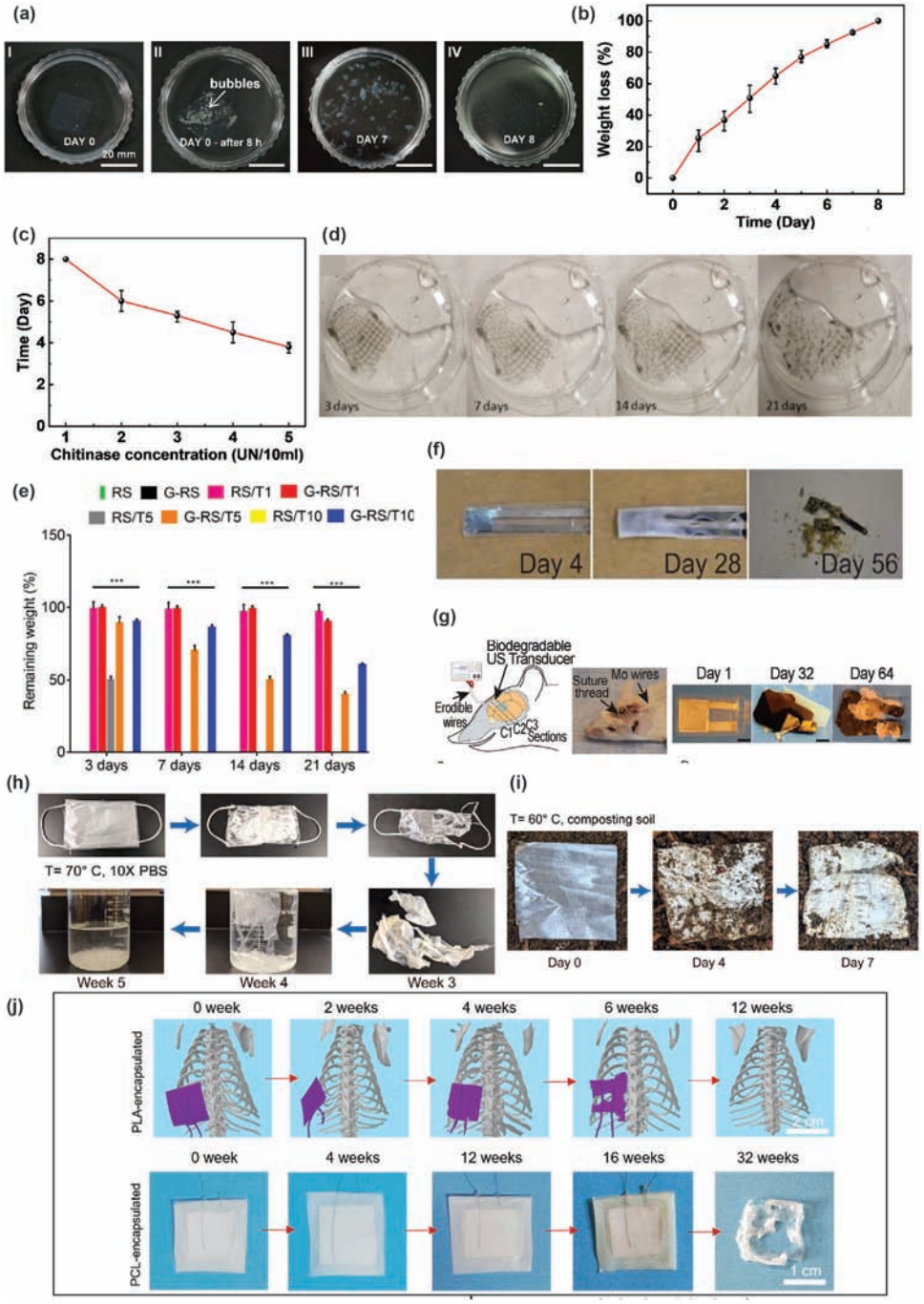

Figure 7. a) Schematics and time-series images of the subsequent phases of biodegradation in the solution of chitinase (1 UN/10 mL). The second phase of the time series shows tiny gas bubbles becoming visible behind the film. b) Effect of time on the weight loss percentage of chitin film (2 × 2) cm^2 in chitinase solution (1 UN/10 mL). c) Effect of chitinase concentration on biodegradation time. Reproduced with permission.[111] Copyright 2018, Elsevier. d) Biodegradable 3D printed composite based on graphene and silk fibroin in PBS solution (i.e., 37 °C. pH 7.4) and e) degradation rate measurements accomplished for the films. Reproduced with permission.[134] Copyright 2022, American Chemical Society. f) Optical photographs depicting the degradability of the sensor in PBS solution on different days at an elevated-decomposition temperature of 74 °C. Reproduced with permission.[22] Copyright 2018, Proceedings of National Academy of Science. g) Optical images showing degradation of US transducer at 70 °C (elevated degradation) temperature at different intervals in PBS solution. Reproduced with permission.[148] Copyright 2020, Proceedings of National Academy of Science. h) Digital photographs presenting the degradation process of the PLLA facemask at an accelerated temperature of 70 °C and concentrated phosphate buffer saline (10× PBS) over time. i) Optical photograms illustrating the degradation of piezoelectric PLLA membranes in compositing soil (with a high temperature 60 °C). Reproduced with permission.[151] Copyright 2022, Wiley-VCH GmbH. j) Biodegradation observation of PLA encapsulated PHBV/PLLA/KNN nanogenerator in vivo via micro-tomography for 12 weeks (top image) and (poly-ϵ-caprolactone) PCL encapsulated PHBV/PLLA/KNN film immersed in PBS solution at 37 °C for 32 weeks (bottom). Reproduced with permission.[149] Copyright 2022, Elsevier.

is needed to fully disclose the piezoelectricity of phage to the lay organization for their potential applications.

4.5. Synthetic Biodegradable Polymers

PLA family has been well studied and utilized as a characteristic synthetic biodegradable polymer. Slow hydrolysis of PLLA was observed when it reacted with water present in the tissue.[190–192] Long term degradation study of high molecular weight PLLA was conducted by implanting it into the back of rats by Bos et al.[193] Mass and molecular weights decreased in the first three months, which was attributed to pure hydrolysis. Additionally, previous research has also examined that an implant based on PLLA could stay for 5.7 years with excellent biocompatibility before being completely degraded by patients.[194] In general, the considerable degradation and piezoelectricity are anticipated to offer more potential in implantable bioelectronics, specifically for in-vivo therapeutics. Curry et al.[22] demonstrated the degradation of PLLA-based piezoelectric force sensors in vivo. The developed sensor fully decomposed and broke into small pieces after 56 days at an elevated decomposition temperature of 74 °C (Figure 7f). They also demonstrated in vivo degradation of the ultrasonic transducer and force sensor made of electrospun PLLA nanofibers. The device worked well for the desired period and was finally self-decomposed (Figure 7g). In a recent study, Le et al.[151] demonstrated the environmentally friendly property of the PLLA membrane. The accelerated biodegradation test was utilized due to the long degradation time of the film. The PLLA membranes were degraded after 5 weeks under the accelerated degradation condition (Figure 7h). Additionally, the PLLA membranes were buried in the soil at 60 °C and minor crack propagation was observed after 7 days (Figure 7i). Wu et al.[149] investigated the degradation behavior of PLA-encapsulated PHBV/PLLA/KNN nanogenerator in vivo through microtomography images (Figure 7j, top) for 12 weeks and poly-ϵ-caprolactone (PCL) encapsulated PHBV/PLLA/KNN piezoelectric film in PBS 37 °C for 32 weeks (Figure 7j, bottom). The device maintained its structural integrity during the first 12 weeks; however, the voltage output of the device was 20% decreased compared to the initial value. After 16 weeks, a remarkable mass loss was observed, and the device was completely degraded during the 32 week time period.

5. Engineering of Piezoelectricity in Biodegradable Polymers

The processing history of any polymer strongly affects its piezoelectric properties. Therefore, to observe piezoelectricity in biodegradable polymers, appropriate processing is needed. Three processing methods are being utilized to sharpen the piezoelectricity in biodegradable polymers apparently: i) thermal annealing (heat treatment), ii) mechanical stretching (drawing), and iii) electrical poling (application of high electric field).

5.1. Thermal Annealing

This method can improve the crystalline part of the amorphous polymer, as presented in **Figure 8**a. Lovell et al.[195] explained the following "Equation (1)":

$$d_{14} = d_a F_a \left(1 - X_c\right) + d_c F_c X_c \quad (1)$$

where d_{14} represents the calculated piezoelectric coefficient, d_a and d_c are the coefficients of piezoelectricity for the amorphous oriented and crystalline regions, respectively, and F_a and F_c represent the orientation functions, respectively, and X_c shows the crystalline fraction. Furukawa, Fukada, and Ando first proposed this expression written in Equation (1) depending on their trials on poly (butylene glutarate) (PBG) and PHB films.[196,197] Figure 8b depicts the positive correlation between the coefficient of piezoelectricity and crystalline fraction in the material.[195] Optically pure PLLA is 30–50% crystalline, and typical temperatures for annealing PLLA are between 80 and 140 °C.[198,199] Although the annealing process is not always advantageous, this treatment improves the orientation of the polymer chains. The annealing process can simultaneously inhibit the dipole's rotation and degrades the material's piezoelectric and ferroelectric features.[200–202] During the thermal annealing process, care must be taken to retain anisotropy. Therefore, thermal annealing is not a good option to get the desired piezoelectric properties. Considering these limitations, further processing is required to maintain anisotropy.

5.2. Mechanical Stretching

Stretching/drawing thin films of polymer uniaxially or biaxially multiple times to its initial length contributes to the alignment of dipoles in one direction.[203] Stretching can be done either at room temperature or high temperature. High-temperature stretching is preferred since it facilitates dipole alignments. Typically, drawing is utilized for inducing or sharpening piezoelectricity in polymeric films. Stretching the polymer can make the chains of polymer in the aligned form in the direction of drawing, thus offering a good anisotropy (Figure 8c).[204] To generate piezoelectricity in various polymers like PLLA, cellulose, collagen, PHB, and polyhydroxy valerate (PHV), parallel ordering of chains present in the polymer is sufficient. Shear piezoelectric coefficient d_{14} was enhanced by applying a ≈5–6 stretch ratio, as presented in Figure 8d.[205] Figure 8e depicts that PLLA shows almost 55% crystallinity at a draw ratio of ≈5–6.[22] Commonly, PLLA is reported in alpha α and β phases. The drawn film of PLLA is comprised of the β phase that is being utilized as biodegradable piezoelectric material.[140] PLLA film with a stretch ratio of 2[205] offered piezoelectricity, whereas the β phase is not observed until stretch ratios of 4 are accomplished.[206,207]

5.3. Electrical Poling

Aligning the dipoles by applying a high electric field is described as electrical poling. This processing is only possible for ferroelectric materials owing to the remnant and spontaneous polarization that can be shifted by applying an electric field. Therefore, polymers containing a ferroelectric phase can be processed by electrical poling. For poling a polymer, electrodes can be directly attached to the material surface or by a corona poling setup (Figure 8f).[208]

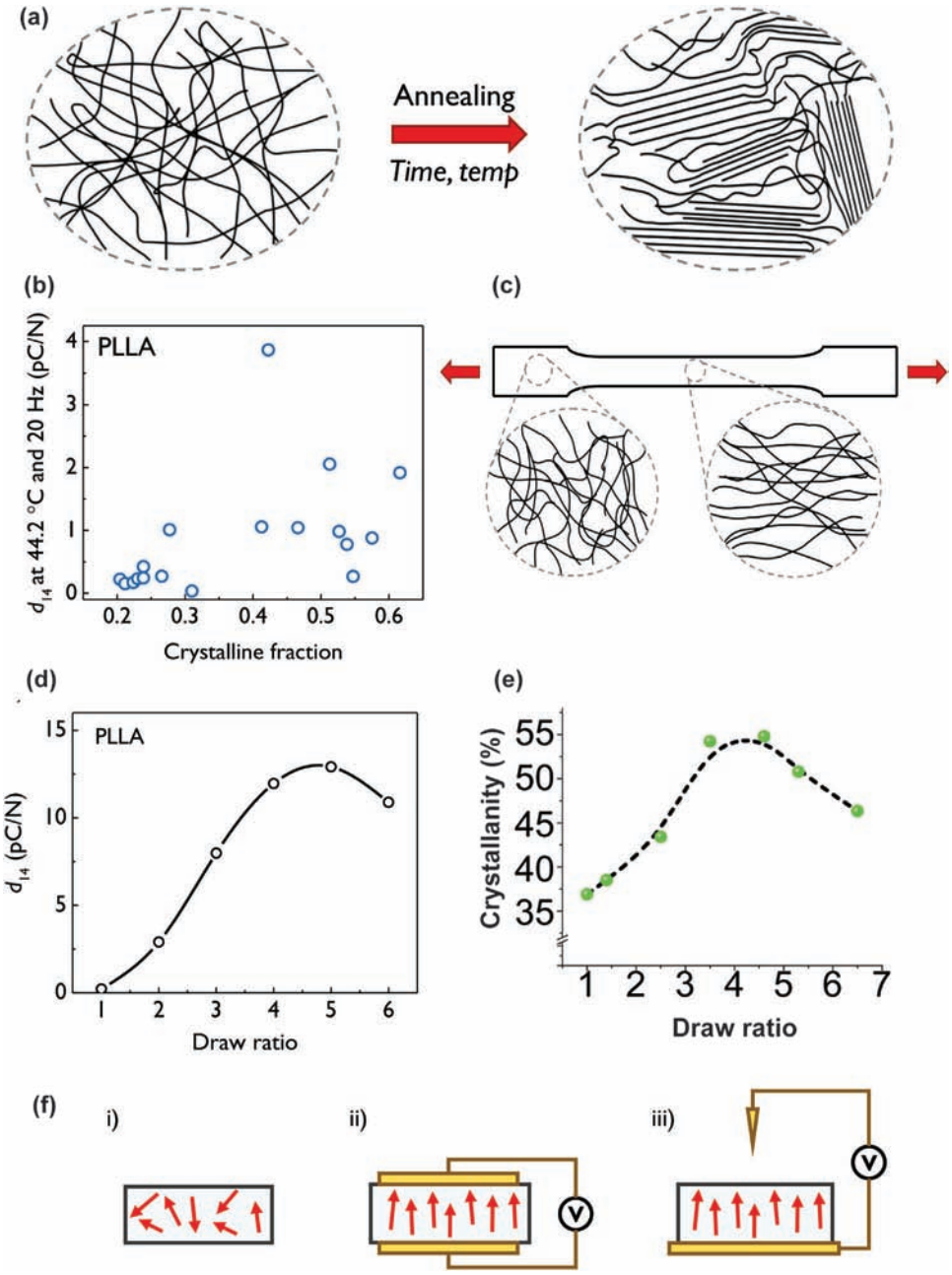

Figure 8. a) A schematic illustration shows the annealing process's effect on polymer crystallization. b) Piezoelectric constant as a function of the crystalline fraction of PLLA. Reproduced with permission.[195] Copyright 2011, Wiley Periodicals, LLC. c) A schematic presentation of the influence of stretching ratio on a polymer specimen. The stretched region shows a considerable degree of orientation. Reproduced with permission.[204] Copyright 1999, Wiley Periodicals, LLC. d) Effect of stretch ratio on the piezoelectric constant of PLLA. Reproduced with permission.[209] Copyright 1995, Elsevier. e) Influence of stretch ratio on the piezoelectricity of PLLA. Reproduced with permission.[22] Copyright 2018, Proceedings of National Academy of Science. f) A schematic showing poling process. i) Dipole moment shown by arrows. ii) Poling by utilizing connected surface electrodes. iii) Corona poling process. Reused with permission.[208] Copyright 2016, Springer Nature.

There are some other methods reported in the literature for increasing the piezoelectricity of biodegradable polymers. For example, Lee et al.[210] prepared diphenylalanine nanotubes (FF) with higher orientation and uni-polarization (**Figure 9**a). Meniscus-driven flow assembly was utilized to develop the nanostructure of FF nanotubes. By adjusting the drawing speeds of the substrates and the percentage of peptide solution, they produced peptide FF nanotubes. Owing to the asymmetric shapes and unidirectional polarization, external forces translated to shear deformation to produce energy.

Nakiri et al.[211] fabricated piezoelectric membranes based on poly-γ-benzyl-L-glutamate (PBLG). They observed high shear piezoelectric constant from a developed membrane oriented by magnetic force. Figure 9b demonstrates the effect of magnetic

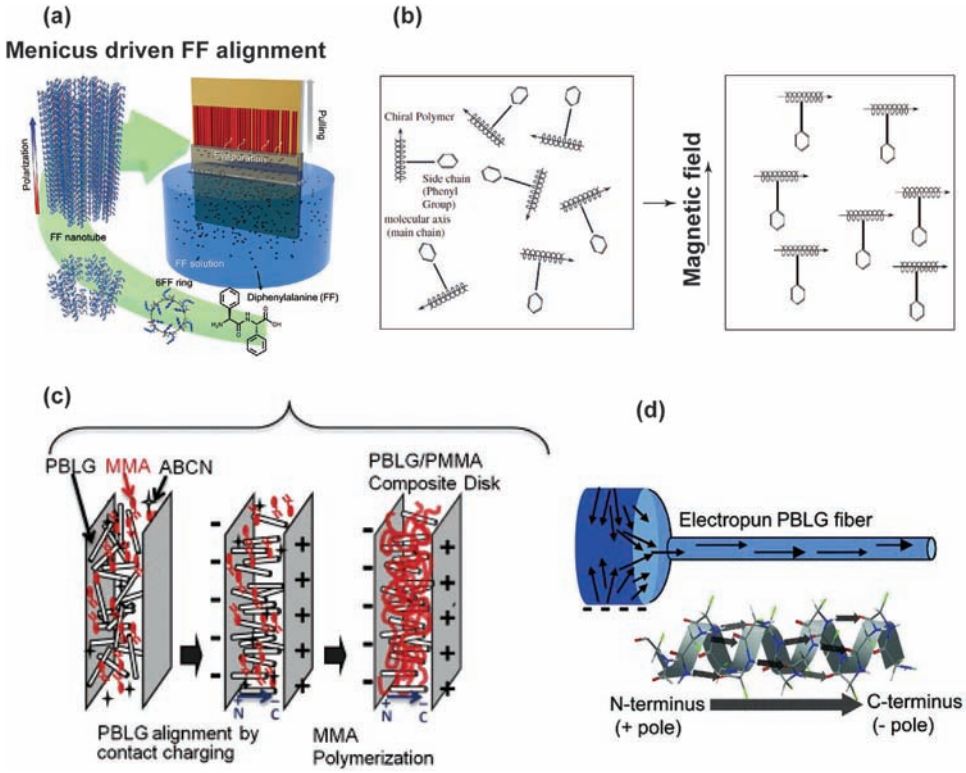

Figure 9. a) Piezoelectric characteristics of FF peptide nanotubes driven by the meniscus. An illustration of the fabrication scheme of making arrays of FF nanotubes with controlled polarization by the meniscus-driven assembly. Reproduced with permission.[210] Copyright 2018, American Chemical Society. b) Schematic demonstration of PBLG molecule's motion under the effect of the magnetic field. Reproduced with permission.[211] Copyright 2004, The Japan Society of Applied Physics. c) Schematic of the α-helical structure of polypeptide molecules (in PBLG-PMMA composite) aligned by corona poling process. Reproduced with permission.[212] Copyright 2011, Elsevier. d) Demonstration of the electrospinning process and α-helical structure of PBLG. Reproduced with permission.[50] Copyright 2011, Wiley-VCH GmbH.

field force on the orientation of PBLG chain molecules. Hwang et al.[212] developed piezoelectric composite material composed of PBLG, poly(methylmethacrylate) (PMMA), and α-amino acid. Piezoelectricity in PBLG was induced by electric poling in the direction perpendicular to the disk's surface. Electric poling of the PBLG layer inside the PMMA matrix resulted in the alignment of PBLG molecular chains (Figure 9c). Farrar et al.[50] used electrospinning for producing high-polarity PBLG nanofibers along the fiber axis. Owing to the rod-like liquid crystal nature of PBLG, the spinning of fiber and high polarity can immediately be linked with an external electric field (Figure 9d).

6. Applications

The biomedical device can function as an actuator, pressure sensor, and other designs that collect bio-physiological signals and detect vital information.[213–215] Biomedical devices are in contact with external or internal tissues, and after their operation, they usually stay in the biological environment, which increases the concern about immunological toxicity or electronic waste. Recently, biomedical devices have been more sustainable and environmentally friendly than old-fashioned non-biodegradable devices. Decomposable piezoelectric-based devices can be designed based on biodegradable materials for advanced biomedical applications.[216–220]

6.1. Pressure Sensor

Biodegradable and piezoelectric polymers exhibit higher flexibility than inorganic materials; thus, they can show deformation under low forces. Due to this property, they can be utilized in applications where they should be conformally wrapped around the curved tissue for measurement. Besides, the biodegradability of the sensor is advantageous in acute and short-term biomedical applications (e.g., wound healing and bone regeneration).

Curry et al.[22] fabricated a force sensor to detect bio-physiological pressures/forces with controlled biodegradability and piezoelectricity. Films of piezoelectric PLLA were made by hot compression molding followed by stretching/drawing and annealing for 8 h at 90 °C. In order to sharpen the device's piezoelectricity, the film of PLLA was cut at 45° angle, concerning the stretching direction. To fabricate a device based on a single layer of piezoelectric material, processed PLLA film was sandwiched between molybdenum electrodes. A sensor design based on multiple layers of processed PLLA is shown in Figure 4a. Deposition of the iron/magnesium combination was done on the film, and it was then folded over and compressed between the electrodes of molybdenum to achieve a multilayer design. After sandwiching the piezoelectric film between electrodes, rectangular sheets of Poly (Lactic acid) (PLA) with a thickness of 100 μm were utilized to cover the sandwiched area, and a PLA-based hot sealing

bag and glue were used to seal the sheets. As demonstrated in Figure 6i, after keeping the sensor at an elevated temperature of 74 °C for 56 days, the sensor exhibited complete degradation. Implantation of a biodegradable piezoelectric PLLA sensor for detecting the diaphragmatic contraction pressure inside the intestinal cavity of the mouse is demonstrated in **Figure 10**a. A distinct pressure response was noticed when the mouse was conscious and breathing under a regular dose of anesthesia. The pressure response was utterly depressed after the mouse overdosed on anesthetics (Figure 10b). The developed device can measure pressure in the range of 0–18 kPa.

Ensieh et al.[65] fabricated a biodegradable piezoelectric pressure sensor based on a thin composite film of chitosan and β-glycine. They reported that growing glycine crystals formed a highly stabilized β-glycine phase in the chitosan matrix to get considerable flexibility in the piezoelectric composite film. Biodegradable and piezoelectric thin film composite was prepared by simple solvent casting. A free-standing composite film was obtained after peeling it off from the petri dish. In the next step, a gold electrode pattern (Au/Ti; 90/10 nm) was deposited using electron beam evaporation and shadow mask method on the top and bottom sides of the composite film. Electric wires were then connected to both sides of deposited electrodes, and Kapton tape was utilized to encapsulate the sensor. It is demonstrated that the sensor can generate an output voltage of 190 mV under pressure (60 kPa) and show sensitivity up to 2.82 ± 0.2 mV kPa^{-1} (Figure 10c). Glycine/chitosan-based pressure sensors could be utilized in biomedical applications for detecting pressure. Moreover, electrical simulations produced from piezoelectric material can contribute to specific tissue regeneration, such as electrical wound healing stimulation. Lu et al.[15] fabricated recyclable and biodegradable force sensor having a sensitivity of 4 mV kPa^{-1}. After applying 0.2 kPa compressive force, it generated an output voltage of 4.5 mV, and the voltage output increased linearly with pressure. This way, pressure levels of 3.75, 7.5, and 31.25 kPa provided 21.3, 39.5, and 140 mV, respectively (Figure 10d).

Curry et al.[148] developed nanofibers based on highly biocompatible and biodegradable PLLA with highly effective, controllable, and stabilized piezoelectric performance. The fabricated device based on the mentioned nanomaterial can easily be implemented in biomedical applications such as biodegradable pressure sensors with high sensitivity for detecting critical bio-physiological pressures. Customized electrospinning techniques were used to fabricate PLLA nanofibers. The already-made nanofibers were post-processed, followed by slow annealing and cooling to increase the nanofibers' crystallinity up to 70–88%. Nanofibers were sandwiched between the molybdenum electrodes from both sides of the nanofibers to fabricate a biodegradable force sensor. For encapsulation of the sensor, untreated layers of PLLA were used. A force sensor (5×5 mm) was implanted inside the abdominal cavity of the mouse to monitor intraabdominal pressure, as demonstrated in Figure 10e. Pressure response from the mouse's abdomen was wirelessly monitored when the mouse's abdomen was periodically compressed and relaxed (Figure 10f). Histology image analysis confirmed the device's biocompatibility inside the mouse's abdomen.

Ensieh et al.[221] developed a biodegradable piezoelectric composite based on chitosan and β-glycine with an efficient piezoelectric response. A simple solution casting method was used to make a film of chitosan/β-glycine composite. The chitosan/β-glycine solution was on a polyimide (PI) flexible substrate coated with the gold (Au), then drying for 2 days at room temperature. After complete drying, another substrate coated with a gold electrode was attached to the other side of the film. A dynamic force/pressure was applied through a shaker on the piezoelectric sensor to measure the suitability of the sensor in pressure-sensing applications. A linear relationship between the output voltage and applied compressive force was observed when the sensor was given force/pressure. The results revealed that the fabricated device could efficiently detect pressure in the range of 0–40 kPa with a sensitivity of up to ≈4.7 mV kPa^{-1}. Machines made of bio-based materials like glycine can provide great potential for healthcare applications, such as a biodegradable wearable device for measuring pressure in a compression bandage. The biodegradable piezoelectric pressure sensor could be utilized to harvest energy from the normal movement of the body parts, thus eradicating the requirement for batteries often needed for conventionally used medical implants. Further, the simple and easy fabrication methods would make the device fabrication more capable for clinical applications.

6.2. Transducers and Actuators

Curry et al.[148] fabricated biodegradable ultrasonic transducer to open the blood-brain barrier, which can be further utilized for drug delivery into the brain. The force sensor developed by curry et al. can also be used as a biodegradable US transducer (Figure 10g). The sensor could show output for different pressures in PBS solution (Figure 10h). The degradation experiment of the US transducer was demonstrated in Figure 8j, showing the survival for 8 days in phosphate buffer saline (PBS) at 37 °C. Figure 10i represents the implantation of a US biodegradable transducer in a mouse skull. The device was observed functioning properly for a pre-specified time and finally self-disposed. Therefore, devices based on PLLA piezoelectric nanofibers could greatly impact different areas of medicine.

Kyungtae et al.[111] fabricated a biodegradable piezoelectric device with highly crystalline transparent film prepared from chitin nanofibers. A bottom-up recreation method was used to make chitin nanofiber films. Silver metal with a thickness of 100 nm was deposited on both sides of the chitin nanofiber film through DC magnetron sputtering system. For the development of a translucent chitin actuator, films of poly(methyl-methacrylate) (PMMA) were spin-coated on each side of the film ((4×6) cm^2), followed by an annealing process for 10 min, at 85 °C. Figure 10j represents chitin-based functional microphones and speakers with oscillated input voltage. The results showed that the chitin microphone recorded and thoroughly sensed harmonic frequencies produced by the chitin speaker. The recorded frequencies from the speaker matched the frequency signal received at the chitin microphone.

Tajitsu et al.[222–224] fabricated an efficient medical catheter based on electrospun nanofibers of PLLA with enhanced piezoelectricity. Subsequently, the top surface of the fiber was coated with two electrodes with a diameter of 40 μm to function as an actuator. The PLLA fiber vibration was observed when AC voltage (50–300 V) was applied at a 0.1–150 Hz frequency. As a result,

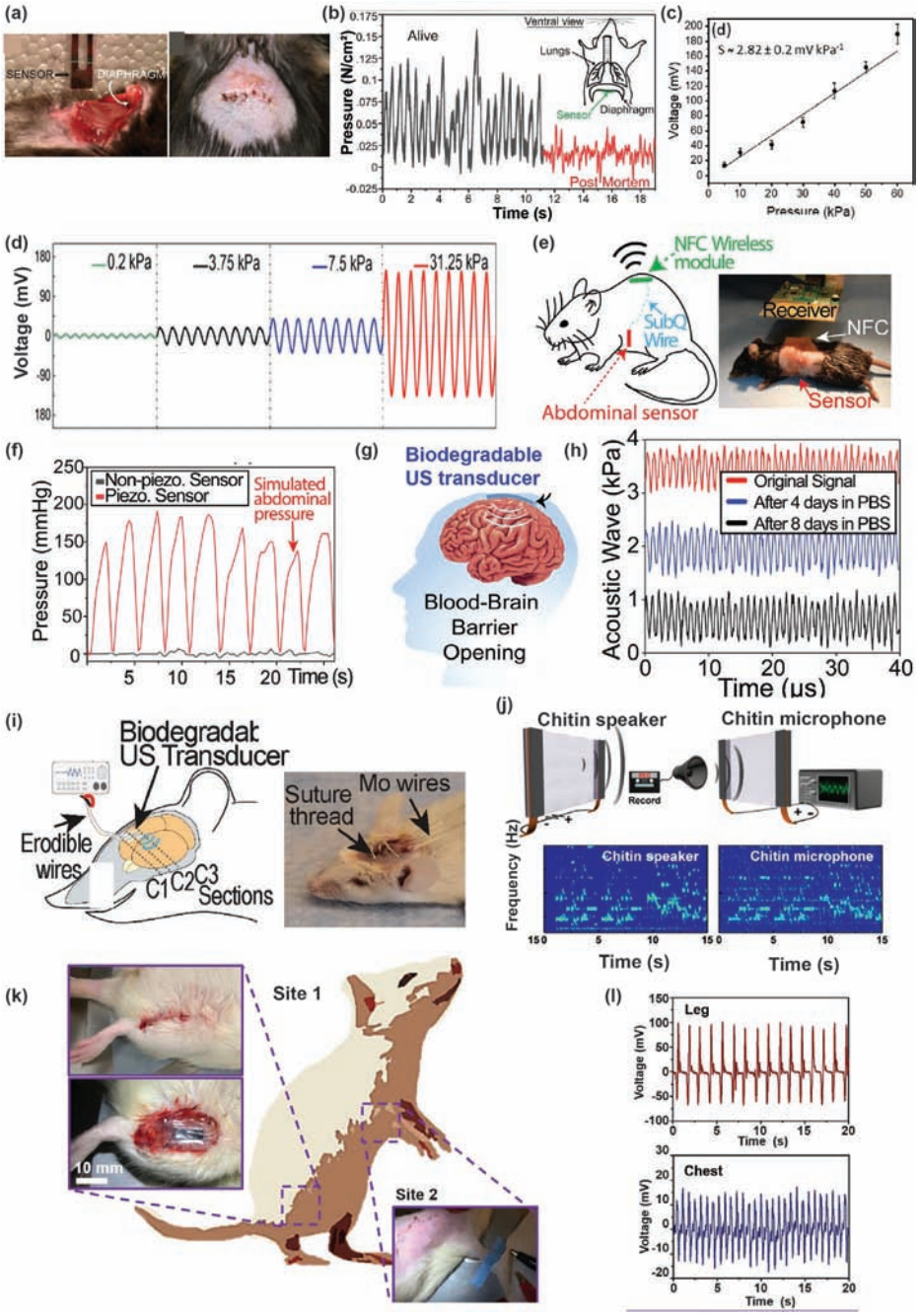

Figure 10. a) Optical photographs depicting the implantation of force sensor for measuring pressure in mouse abdominal cavity (left) and sealing of wound by medical suture on mouse abdomen in which PLLA sensor was implanted (right). b) Signals are produced by the implanted sensor under anesthesia and alive (black) and euthanized state (red). Reproduced with permission.[22] Copyright 2018, Proceedings of National Academy of Science. c) Piezoelectric sensitivity of Chitosan/glycine-based sensor with respect to applied pressure. Reproduced with permission.[65] Copyright 2020, American Chemical Society. d) Output voltage under the effect of different pressures of 0.2, 3.75, 7.5, and 31.25 kPa. Reproduced with permission.[15] Copyright 2022, American Chemical Society. e) A schematic showing the wireless pressure sensor and its presence in the mouse (left). Optical photo of the mouse and communication through NFC (right). f) Comparison between the pressure values obtained from implanted PLLA sensor using piezo (4000 rpm film, red) and non-piezo sensor (300 rpm film, black). g) A simplified schematic displays the implanted ultrasonic transducer inside the brain, which can continuously generate ultrasound to deliver the drug to the brain and open the blood-brain barrier. h) Pressure output signals were received from a biodegradable US transducer on different days. i) A schematic (left) and optical photo of (right) implantation for in vivo experiment to demonstrate the capability of the US transducer for drug delivery and the blood-brain barrier. Reproduced with permission.[148] Copyright 2020, Proceedings of National Academy of Science. j) Schematic sensor demonstrations based on chitin as chitin speaker and microphone. Reproduced with permission.[111] Copyright 2018, Elsevier. k) Schematic illustration and optical images of implanted glycine-PVA packaged films in the chest and thigh of SD rats. l) Voltage output response from the piezoelectric glycine-PVA film inserted on the quadriceps femoris muscle thigh at the thigh area while gentle stretching. Reproduced with permission.[51] Copyright 2021, AAAS.

the fabricated PLLA fiber-based medical tweezer could gasp and eliminate a sample of thrombosis. Additionally, the capability of moving blood in vessels was demonstrated.

In recent studies, Yang et al.[51] proposed a self-assembly-based and wafer-scale approach to fabricate a PVA-glycine-PVA sandwich structure. They demonstrated the potential applications of the developed biodegradable piezoelectric film in biological systems. The glycine-PVA film packaged with PLA was implanted in vivo in Sprague–Dawley (SD) rats (Figure 10k). The developed novel bioresorbable piezoelectric material exhibited impressive piezoelectric response in-vivo when glycine-PVA was implanted in the chest and thigh (Figure 10l). Owing to the degradability and natural compatibility of glycine-PVA composite film in a physiological environment, it may facilitate the development of new transient implantable devices such as transducers and actuators. Joseph et al.[225] fabricated a piezoelectric micromachined ultrasonic transducer (PMUT) based on bioresorbable piezoelectric silk. They demonstrated that an ultra-smooth thin (roughness = 2.84 nm, d_{33} = 56.2 pm V^{-1}) film of silk containing natural piezoelectricity was used as a piezoelectric component of the PMUT. When tested in air, the developed device exhibited a fractional bandwidth of 3.18% at the center frequency of 76.59 kHz. They claimed that silk piezoelectric thin film has great potential in PMUT applications. Marzo et al.[226] reported a facile approach for the fabrication of an ultrasonic transducer using a biodegradable piezoelectric thin film of chitosan. Their work represents the future development of fully degradable, flexible, transparent, and thin piezoelectric micro-transducers. The most critical factors for actuator and transducer devices are biocompatibility and degradability and simultaneously performing effectively. Thus, the more utilization of these bioresorbable piezoelectric materials in tissue engineering devices,[215] efficient antibacterial textiles,[227] and intelligent monitoring devices[228,229] are now turning into the popular strategy to enable biodegradability and biocompatibility while keeping the desired performance.

6.3. Physiological Signal Monitoring

Collagen[126,230] and silk[106,178] based piezoelectric devices have been recently investigated as potential candidates as sensors in the human physiological system. A piezoelectric-based electronic skin inspired by fish skin comprised of nanofibrils of collagen[126] and natural silk[159] based was demonstrated in the literature. Sultana et al.[165] fabricated bio-e-skin based on electrospun PLLA nanofibers for monitoring non-invasive physiological signals. They reported that the sensor could monitor human physiological signals, monitor sports performance, and recognize the voice. This sensor was placed on the wrist to demonstrate its applicability for monitoring sports performance (**Figure 11**a). While bending the wrist, PBio-e-skin experienced more static strain leading to the production of current signals. Figure 11b displays the recent response from bending and relaxing the wrist. PBio-e-skin sensor was also attached to the carotid artery under the neck (Figure 11c), and a current response was noticed over the pulse period (Figure 11d). The developed device could be used in various applications, including prosthetic skin, artificial intelligence, human-machine interfacing systems, and wearable health care systems. Sujoy et al.[55] a designed self-powered wearable device for detecting non-invasive human physiological signals based on prawn shells. They demonstrated the device's functionality by measuring critical non-invasive and high-fidelity signs, such as coughing and pulse waves. They attached the sensor to the wrist with the help of adhesive tape (Inset of Figure 11e). When the wrist was bent and relaxed, a clear current pattern was generated owing to the stretching and shrinking movements of the body. They demonstrated the functionality of the fish skin-based sensor by recording coughing actions. The sensor was found to work with reasonable accuracy in monitoring the vocal cord vibrations (Figure 11f). In addition, a sensor was also placed just over the radial artery (inset of Figure 9g). The real-time response the sensor shows under normal conditions is illustrated in Figure 11g. Maiti et al.[106] developed a novel biodegradable piezoelectric device using onion skin containing inherently self-organized cellulose fibers was reported. The onion skin-based piezoelectric device successfully detected speech signals demonstrating its ability to recognize speech. The fabricated device was found efficient in detecting the movement of the throat while swallowing, coughing, and drinking. It could be further utilized in health care units and pacemakers. In a study by Li et al.,[232] a biodegradable nanogenerator based on PLLA and vitamin B2 was utilized as an interactive controlling system and wearable sensor. The ability of energy harvesting of the PLLA-VB2 nanogenerator was demonstrated by attaching the device to the finger and elbow. Increasing the frequency of joint movement enhances the response in the output voltage. Further, an onion skin-based bio piezoelectric device exhibited high sensitivity in detecting human body motions such as heel pressing (Figure 11h) and wrist movements (Figure 11i).

Le et al.[151] developed humidity-resistant air filtration membranes using highly stable and controllable piezoelectric electrospun nanofibers of PLLA. The fabricated membrane exhibited a desirable pressure drop (≈91 Pa at normal condition) while possessing high filtration efficiency (>91% for PM 1.0 and > 99% for PM 2.5). They demonstrated that the PLLA filtration mask is reusable through common disinfection tools, including microwave, autoclave, and ultrasonic cleaning bath. To prove the significance of the environmentally friendly feature of the fabricated filter membrane, they constructed the first prototype of a fully bioresorbable piezoelectric facemask (Figure 11j). In brief, bioresorbable piezoelectric materials could have great potential for filtering contaminated/polluted air, inhibiting the transmission of dangerous viruses, and resolving critical environmental crises.

6.4. Tissue Engineering

Bioresorbable piezoelectric polymers are an attractive option for tissue engineering applications owing to their simultaneous biocompatibility and piezoelectric properties with minimal toxicity. The bioelectric signals produced by piezoelectric scaffolds improve the physiological electric environment regulating the action of cells towards effective bone regeneration and repair.[233,234] The widely studied piezoelectric polymers for bone tissue engineering (BTE) are PVDF, its copolymers, and PLLA. However, there are some major constraints regarding the utilization of PVDF in BTE because of its non-degradability, resulting in

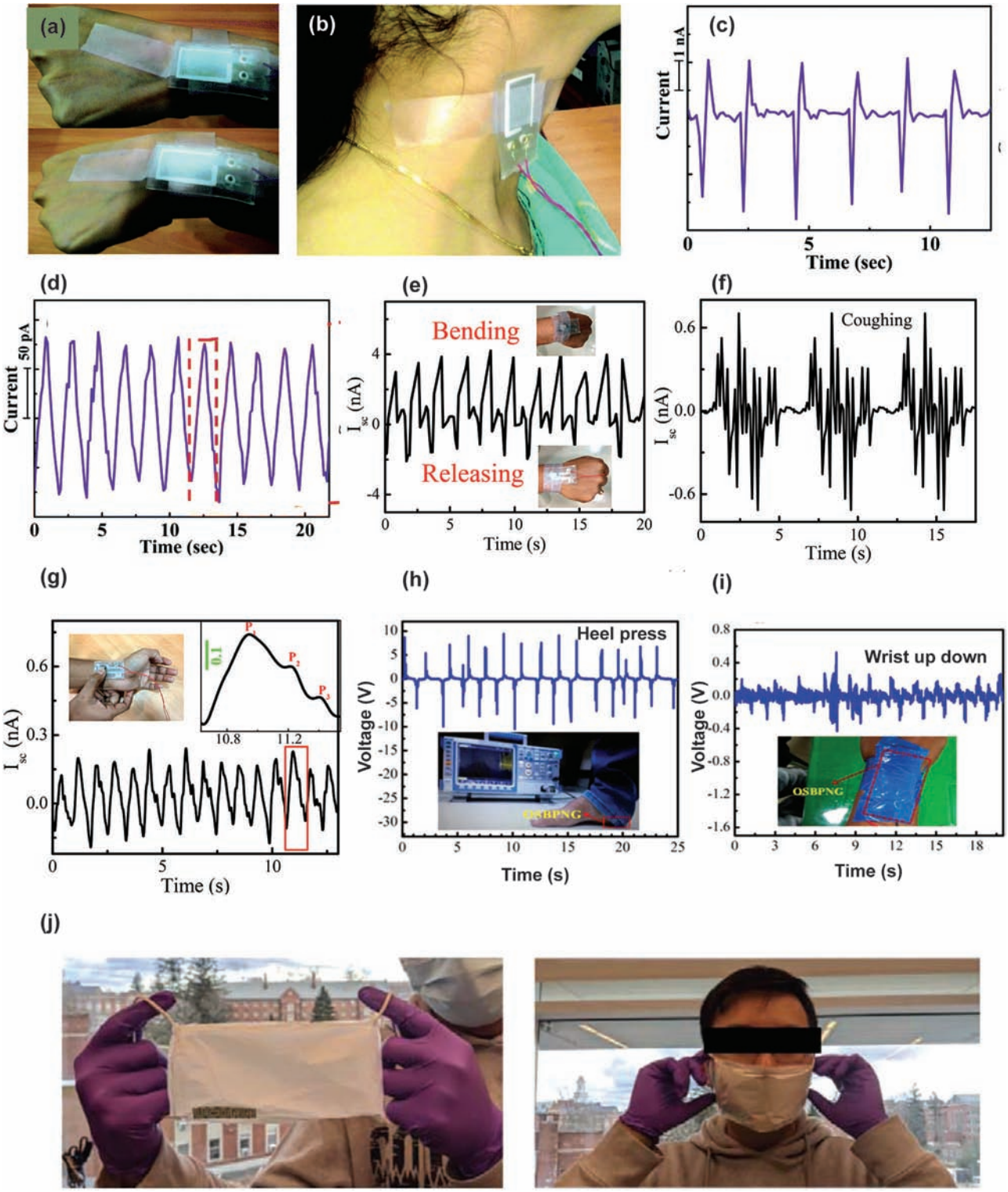

Figure 11. a) Optical image of bio-e-skin attached to the wrist joint. b) Photograph displaying that the sensor is placed under the neck for monitoring the carotid artery. c) Output current obtained as a result of wrist motion. d) Real-time measurement of current output obtained by the sensor attached to the carotid artery. Reproduced with permission.[165] Copyright 2017, Royal Society of Chemistry. e) Real-time monitoring of time-dependent current from continuously bending and releasing the wrist. f) Coughing action and g) Radial artery. Reproduced with permission.[126] Copyright 2017, American Chemical Society. h,i) Output voltage as a function of time for detecting motions in: h) heel pressing, i) wrist bending, and stretching. Reproduced with permission.[106] Copyright 2017, Elsevier. j) The fully bioresorbable facemask prototype was developed using piezoelectric PLLA nanofibers. Reproduced with permission.[151] Copyright 2022, Wiley-VCH GmbH.

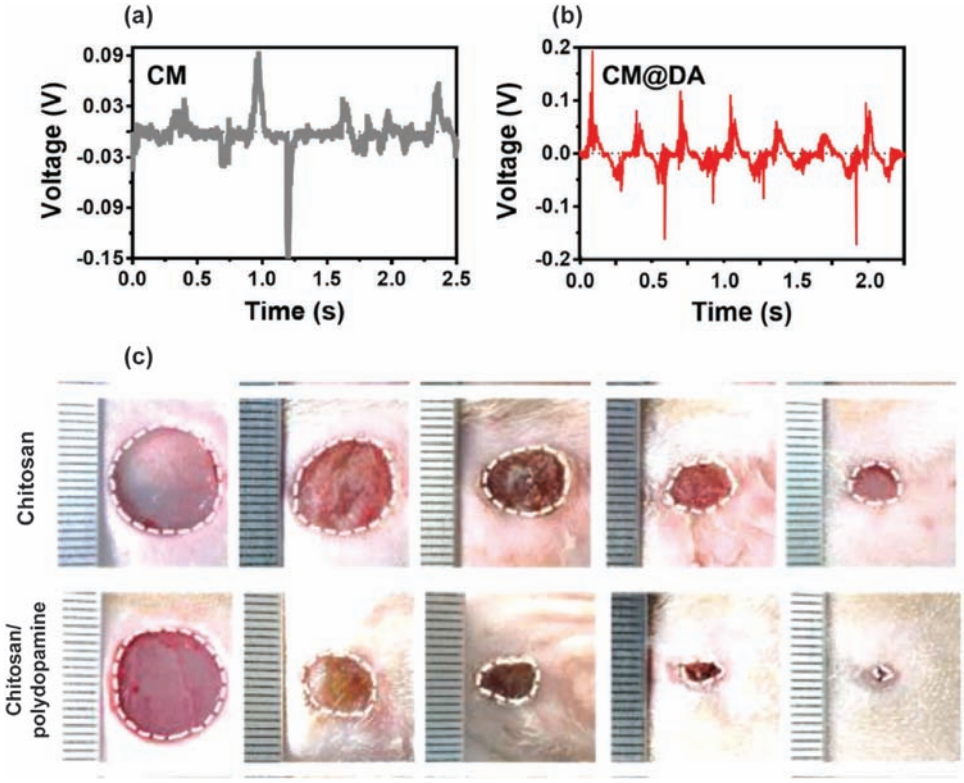

Figure 12. The in vivo output voltage was obtained for a) chitosan and b) chitosan/polydopamine after attaching them to the dorsal parts of SD rats. c) Optical photographs of wounds at days 0, 4, 7, 10, and 14 after different treatments. The scale bar of the images is equal to 1 mm. Reproduced with permission.[240] Copyright 2020, Elsevier.

natural polymers, polyesters, and polyhydroxyalkanoates being preferred.

Natural bioresorbable piezoelectric polymers, including cellulose, collagen, silk, etc., have been investigated to heal nerve conduits. For instance, a nerve guide fabricated using collagen biomaterial via a freeze-drawing process enhanced Schwann cells' alignment and migration.[235] The chitosan/collagen composite resulted in the formation of scaffolds with controlled swelling rate, pore size, and in-vivo degradation.[236] Silva et al.[237] developed a bioresorbable piezoelectric biomaterial composite based on anionic collagen and hydroxyapatite (HA). The fabricated composite showed the potential to be utilized for bone regeneration and cellular growth. The piezoelectricity value of collagen-HA membranes was around 0.042 pC N^{-1}. Chitosan is another natural bioresorbable piezoelectric polymer utilized for nerve tissue engineering (TE). The conduits made of chitosan have been demonstrated to fill sciatic nerve gaps in vivo, leading to the regeneration of axonal and remyelination in the bridged nerves.[236,238] The piezoelectricity of chitosan speed up the wound-healing process. Specifically, it promotes tissue formation and fosters angiogenesis and normal deposition of collagen fibers.[239] Chen et al.[240] demonstrated accelerated wound healing using the piezoelectric property of the chitosan-polydopamine composite film. The fabricated composite film generated large piezoelectric voltage in response to the rats' movement, leading to quick wound healing (**Figure 12**). In addition, combining keratin and gelatin enhanced the piezoelectric properties, permitted better cell migration and spreading, and better re-epithelialization than pure gelatin.[241] Furthermore, the combined piezoelectricity produced by cellulose and chitosan composite enhanced regeneration and epithelial formation.[242]

Several studies have also been conducted to utilize synthetic biodegradable and biocompatible piezoelectric polymers, such as PLLA, as tissue stimulators to improve the differentiation and proliferation of cells. Stretched/drawn rods of PLLA implanted in the intramedullary space of the feline tibia of cats form considerable calluses compared to unstretched rods of non-piezoelectric PLLA.[243] Callus formation was increased with the increase in the stretch ratio of the PLLA rod, resulting in improved fracture healing. The findings of this study pinpoint that the stretched PLLA enhances the device functionality for fracture fixation. Additionally, the resorbable nature of PLLA in the body removes the need for a second surgery.

Ramasamy et al.[244] reported a new method to fabricate poly(L-lactic acid) nanofibers (PLF) with good cytocompatibility, enhanced surface properties, and improved piezoelectricity using electrospinning with carbon nanomaterial (CM) and polydopamine (PD) coating strategies. The results of this study demonstrated that the fabricated scaffolds of PLF with tunable surface and piezoelectric properties could offer energetic extracellular microenvironments to speed up the tissue regeneration and healing process. **Figure 13**a presents a qualitative live/dead viability staining assay analysis. The live (green) and dead (red) fibroblasts can be seen on the live/dead staining assay.

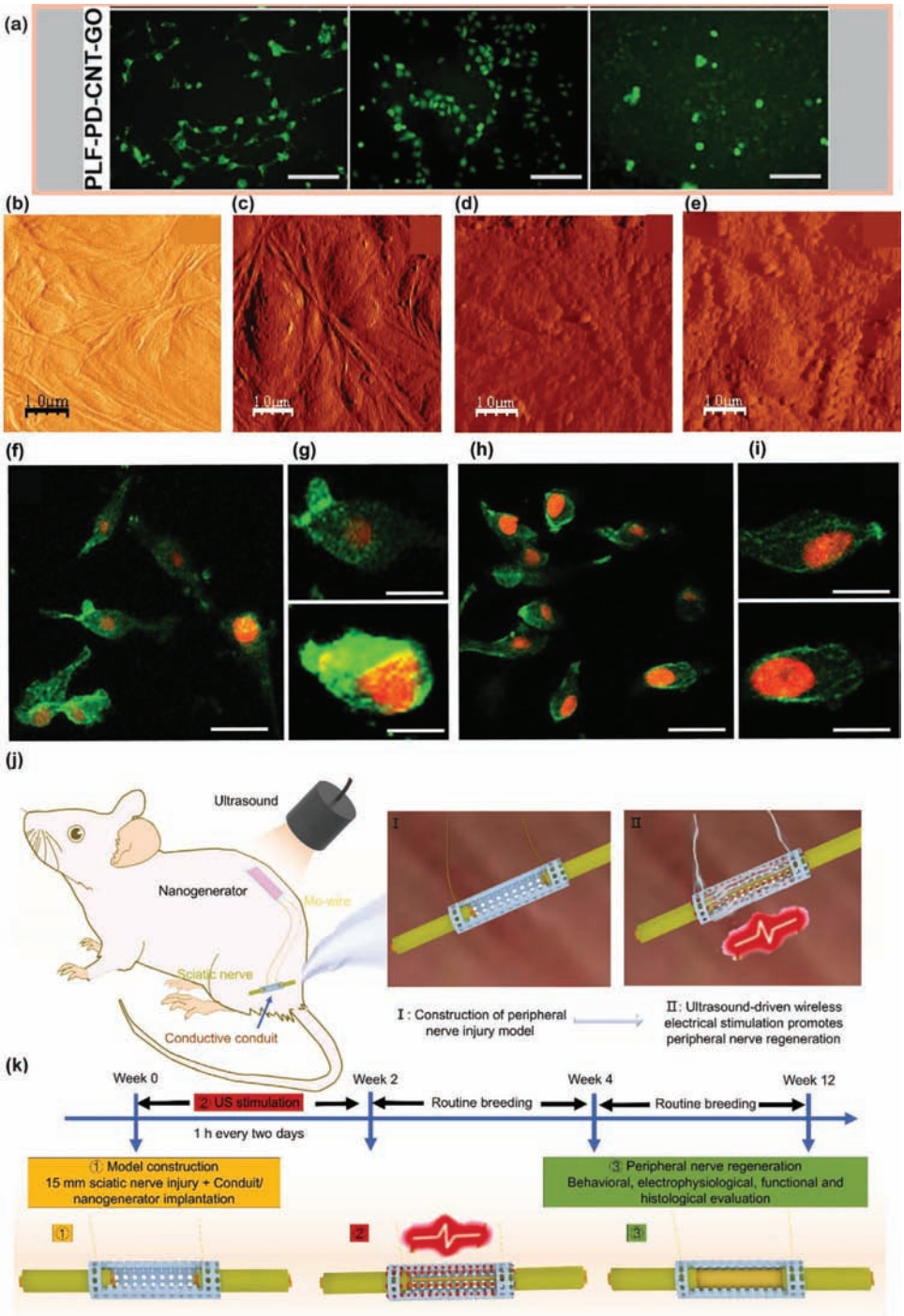

Figure 13. a) Live/dead staining assay conducted for days 1, 3, and 5 on PLF scaffolds coated with PD-CM. Reproduced with permission.[244] Copyright 2022, Elsevier. b–e) Photographs of PLLA thin films obtained by using AFM b) unpolarized area before the adsorption of protein, c) unpolarized area after the adsorption of protein, d) positively polarized area after the adsorption of protein e) negatively polarized area after the adsorption of protein. Reproduced with permission.[246] Copyright 2011, AIP Publishing LLC. f–i) Images acquired from confocal laser microscopy for osteoblastic MG-63 cells cultivated on PLLA (f,g) and gHA-PLLA films (h,i) for 24 h. Reproduced with permission.[247] Copyright 2017, Elsevier. j) Schematic image of implanted PHBV/PLLA/KNN film nanogenerator combined with ultrasound to deliver in vivo electrical stimulation to enrich the peripheral nerve repair. k) The scheme of enhancing the healing process of impaired peripheral nerves by ultrasound-driven wireless electrical stimulation. Reproduced with permission.[149] Copyright 2022, Elsevier.

Table 2. Few scaffolds used for skeletal regeneration.

Scaffolds	Impact on skeletal repair
Crosslinked electrospun PLLA/collagen[252]	Expedite the growth of human fibroblasts.
Electrospun PLLA[253]	Highly organized fibers of PLLA, as compared to random fibers of PLLA, led to dense tendon-like tissues forming.
Electrospun PHB and PHBV[254]	The improved piezoelectricity coefficient d_{33} enhanced the gene expressions, proliferation, and chondrocyte adhesion.
PLLA braided scaffolds[255]	Upregulation of *sox2* and *oct3/4* genes.
Electrospun PLLA[256]	Stimulated in-vivo bone regeneration in a critical-size calvarial defect and improved the in-vitro osteogenic differentiation of stem cells.
Electrospun bacterial cellulose[257]	Promoted the adherence and migration of fibroblasts and prevented the growth of epidural scars, hyperproliferation of muscle, and cerebrospinal fluid leakage.

Incorporating PD-CM into the PLF scaffolds remarkably enhanced the cytocompatibility and permitted the proliferation and adherence of fibroblast. The PLF scaffolds coated with PD-CM represent a qualitatively large number of live cells compared to PLF scaffolds after five days of culture.

Poled piezoelectric PLLA exhibits higher protein absorption and improves proliferation and cellular adhesion[245,246] which is advantageous for tissue regeneration. Figure 13b–e presents four different films of PLLA revealing atomic force microscopy (AFM) results. It confirms that a considerably good quantity of proteins was immersed in poled PLLA sample. Notably, improved proliferation and adhesion of cell was noticed in negatively poled PLLA. However, results from the protein absorption test revealed that poled surface could change the orientation or conformation of the absorbing proteins, which may impede or reveal their cell-binding areas.

Santos et al.[247] developed electrospun micro-composite membranes made of glass-reinforced hydroxyapatite micrometer granules (gHA) as filler and PLLA as a matrix for the improvement in the regeneration of bone tissue. Membranes of gHA-PLLA and PLLA were obtained with the help of an electrospinning setup. The growth of osteoblastic cells was noticed on composite membranes, and on day 1, samples of gHA-PLLA membrane demonstrated an increased spreading of the cells compared with membranes made of PLLA (Figure 13f–i**)**. Micro-composite based on gHA-PLLA could be suitable for bone healing applications as they improve alkaline phosphatase activity and permit improved F-actin cytoskeleton organization.

Recently, Wu et al.[149] developed an ultrasonic-driven bioresorbable piezoelectric nanogenerator for accelerating the damaged nerve tissues healing period. This device was built by utilizing fully biodegradable piezoelectric poly(3-hydroxybutyrate-*co*-3-hydroxy valerate) (PHBV)/Poly (lactic acid) (PLLA)/potassium sodium niobate (KNN) as a functional layer. To demonstrate the potential of the developed nanogenerator to enhance nerve regeneration in vivo, the nanogenerator encapsulated with PLA was connected to HEC/SPI/BP (HSB) nerve conduit from both ends with molybdenum (Mo) wires and wireless electrical simulation driven by ultrasound was applied to the conduit to enhance nerve healing (Figure 13j). This biodegradable piezoelectric nanogenerator has the potential to be implanted as a neuro-stimulator providing dynamic feedback response to evaluate the nerve repair progress. A schematic shown in Figure 12l briefly explains the method of healing the injured peripheral nerves with the help of electrical stimulation driven by ultrasound. The findings of this study would initiate a new route to introduce electrical cues to nerve healing in a minimally invasive and wireless fashion.

Gorodzha et al.[248] stated that piezoelectric scaffold based on poly(hydroxybutyrate-*co*-valerate) (PHBV) effectively mimicked the growth of bone and improved the differentiation of human mesenchymal stem cells (MSCs) into osteoblasts. The inclusion of hydroxyapatite (HA) and polyhydroxyalkanoates (PHAs) into piezoelectric polymers resulted in better osteoblasts proliferation, spreading, adherence, and alkaline phosphatase (ALP) activity.[249,250] A scaffold based on PLLA/collagen/HA demonstrated higher mineralization and proliferation for the growth of human fetal osteoblasts compared to PLLA and PLLA/HA scaffolds. This can be attributed to the increased piezoelectricity due to the fiber alignment due to the addition of HA and collagen.[251] **Table 2** summarizes some piezoelectric polymer scaffolds demonstrated for skeletal regeneration.

To date, tissue engineering scaffolds based on the effect of piezoelectricity needed dynamic loading to produce electric charges. This could be a bottleneck in the direction of their clinical translation. Indeed, if overcome, bioresorbable piezoelectric materials may become commonly used for biomedical applications. Some investigations reported ultrasound-driven piezoelectricity in scaffolds.[149,258] However, it may negatively impact the cells because of the other physical effects including the need for acoustic streaming, radiation force, cavitation, and heat generation. Biodegradable piezoelectric materials with considerable piezoelectric output could be tuned regarding microstructure and physiochemical properties, resulting in a desired scaffold design. On the contrary, their full potential has not been studied, and a new bioreactor concept should be designed to mimic mechanical conditions in-vivo. To achieve this design, a bioreactor culture for the implantation of the cells and pre-differentiation can be developed based on piezoelectric stimulation.

6.5. Nanogenerators for Energy Harvesting Applications

Due to the electromechanical coupling, the biodegradable piezoelectric nanogenerators can function as piezoelectric nanogenerators. FF peptide nanotube is considered an efficient material for its applications in energy harvesting[36,78,80–83] as it has piezoelectricity almost comparable to commercially used piezoelectric materials such as PVDF.[259] Nguyen et al.[83] fabricated green energy harvester based on peptide nanotubes. Under 60 N force, sensor-generated short circuit current (I_{sc}) of 39.2 nA, the output voltage

of 1.4 V, and power density of 3.3 nW cm^{-2}. The developed nanogenerator-operated liquid crystal display (LCD) exhibits its potential to be used as a power supply.

Another energy harvester based on highly aligned large-scale nanotubes was developed by Lee et al.[210] FF nanotubes were observed to show good piezoelectricity (e.g., $d_{15} = 46.6$ pm V^{-1}). An output voltage of 2.8 V, short circuit current (I_{sc}) of 37.4 nA, and 8.2 nW of power were obtained by applying 42 N of force, which could operate an LCD panel. Another biomaterial, "Virus," was investigated as a promising material for energy harvesting due to its chemical modification ability. Shin et al.[139] used nanopillars of vertically aligned M13 bacteriophage for fabricating a piezoelectric nanogenerator. Short circuit current (I_{sc}) of 11.1 nA and 232 mV of output voltage was obtained when a force of 30 N was applied to the nanogenerator. With a load resistance of 10 MΩ, the power output was 0.9 nW. Although the power output of the nanogenerator was low compared to peptide-based devices, it could still be utilized for tiny sensor nodes. Lee et al.[164] recently introduced power generators based on virus material improved piezoelectricity by creating better dipole alignment. The fabricated device could operate LCD panels and lighten up commercial LEDs, showing promising potential as a power source for small batteries.

In summary, piezoelectric nanogenerators based on biodegradable materials could produce electricity at the nano level. Although power output from these materials might not be comparable to other energy harvesters, for instance, triboelectric[260–263] and electromagnetic generators.[264–266] However, a novel thing about these piezoelectric biomaterials is to use them with biodegradable electrodes (i.e., conducting polymers, magnesium, iron) and biodegradable encapsulation layer (i.e., PLGA, PCL, PLA) to fabricate novel biodegradable implantable devices.[218]

7. Conclusion and Future Outlook

This report thoroughly covered the most recent literature progress in the development of bioresorbable piezoelectric polymers. Here, we emphasized fabrication and structural material development, followed by their piezoelectricity degradation mechanisms. Major types of natural and synthetic biodegradable piezoelectric polymers are discussed. Furthermore, the most recent and novel applications of bioresorbable piezoelectric polymers in biomedical devices are systematically represented. Regardless of the efforts and growing research interests, the development of natural and synthetic bio-piezoelectric polymers and their applications in the medical field are still emerging. Despite having all these intriguing potential abilities, both synthetic and nature-derived polymers are still experiencing challenges below:

1) Long-term stability has excellent importance for biodecomposable piezoelectric polymers. Polymorphs of most of the amino acid-based polymers having considerable piezoelectricity are metastable. For instance, transformation of β-glycine to γ and α-glycine occurs at room temperature. Moreover, several biomedical devices must pass through several strain cycles, reducing the piezoelectric performance of peptides-based polymers containing low stability. In addition, high temperature is of great concern for most biological materials as they cannot continuously exist in harsh environments. Using synthetic PLLA above 60 °C could also be problematic as its low glass transition temperature is at ≈60 °C.[267,268] A solution to this problem could be a strong encapsulation layer that can improve stability and durability.

To get a higher piezoelectric response, more efficient methods must be followed to control polarization in biomaterials. Although capillary and shear forces could improve the orientation of molecules, these mechanical forces offer weak polarization, which may result in the antiparallel conformation of polar groups. Nevertheless, dipole moment and direction could be controlled well by utilizing reasonable methods, including electrical and mechanical forces that may eventually result in optimal performance. We envisage two levels of upgrading that may result in addressing this challenge. Optimized structure design and an effective alignment approach at the macroscopic level are promising methods to upgrade the piezoelectric performance. Modulating the molecules of biomaterials on a molecular level is another effective way to enhance intrinsic piezoelectric polarization. Major types of natural bio-piezoelectric material consist of rich functional groups and can combine with other ions.[269–272] This feature permits researchers to make additional changes to the molecular assembly and improve the overall polarization. For instance, in a recent study, using confinement cell technology, the design of colloidal opal structures for the alignment of cellulose nanocrystal rods vertically on a large scale.[39]

2) Exact methods should be established to measure the piezoelectric performance of biodegradable piezoelectric materials to avoid measurements from other factors. For instance, the piezoelectricity of collagen and cellulose biomaterials may change over time with a high order of magnitude.[125] Because of different measurement techniques, the presence of a number of polymorphs and other influences from electromechanical coupling might affect the results.
3) Biodegradable piezoelectric materials reported up till now are stiff and rigid compared to organs and human skin. For example, Young's modulus of synthetic PLLA is in GPa,[273,274] and it is ≈19 GPa for self-assembled peptides.[73] Some collagens could have Young's modulus range of 20–200 MPa.[275,276] However, it is still more than the soft tissues. Further, there is always a conflict in getting higher piezoelectric output with simultaneously having softness and flexibility, as flexibility and softness comes from the amorphous nature of the polymer. In contrast, the high crystallinity of the polymer shows more piezoelectricity. Therefore, keeping the piezoelectricity high while simultaneously enabling biomaterials' biomimetic properties could be a great challenge for future wearable and implantable devices. Limited polarization, orientation control, and patterning directions are also critical challenges for developing bioresorbable piezoelectric materials. To overcome these challenges, 3D printing, inkjet printing, and electric and magnetic field-induced alignment methods have been utilized.[81,83,164,277–280]

Unlike solid shear components, most synthetic and natural biodegradable piezoelectric materials show weak longitudinal

and transverse responses. For example, the piezoelectricity of β-glycine is lower in the longitudinal one (4.7 pC N^{-1}) than piezoelectricity in shear mode (179 pC N^{-1}). Some highly organized materials only display shear piezoelectricity. Nonetheless, normal out-of-plane stress is considered the most frequently used mechanical stimuli. Therefore, the device should be designed so that normal out-of-plane stress can be translated into in-plane shear, which may result in complicated fabrication and lower efficiency.

4) Many of the applications of biodegradable piezoelectric polymers, including scaffolds, sensors, nanogenerators, and ultrasonic transducers, all need bulk-scale material building blocks. To develop more practical devices, it is necessary to introduce effective techniques for fabricating high-quality bioresorbable piezoelectric materials. Evolving processes, such as additive manufacturing, are anticipated to offer much ease in material preparation and device manufacturing. Utilizing machine learning advances and state-of-the-art data science, we may introduce more instructive blueprints for the preparation of materials.
5) Several bioresorbable piezoelectric polymers are inherently soft and are in the form of nanomaterials. Precise measurement of piezoelectric properties of biodegradable piezoelectric nanomaterials is an intricate process, but it is considered a key factor for selecting a suitable material for specific biomedical applications. Recently, Rodrigues et al.[35] reported an experimental design for quantifying the piezoelectric coefficient of chemically modified graphene nanoparticles. They deposited a single graphene layer onto the silicon dioxide (SiO_2) substrate. The findings of this study revealed that chemical interaction between the substrate's oxygen atoms and graphene's carbon atoms resulted in inducing non-zero net dipole moment and polarization in the examined system. Based on this study, piezo force microscopy (PFM) measurements were performed to characterize the piezoelectricity of nanomaterial. One of the most reliable and promising methods for quantifying and detecting piezoelectric properties of nanomaterials is PFM.[281] This method of piezoelectric characterization has been studied recently, becoming an appropriate technology at the micro and nanoscale.[282] Owing to the possibility of measuring the local piezoelectricity in nanomaterials with non-uniform geometries, nondestructive imaging ability, and high resolution, PFM has become a widely used tool for measuring piezoelectricity at the nanoscale. The typical PFM modality utilizes the indirect piezoelectric effect. However, in recent times, there have been improvements regarding using direct effects to infer electrical signals from nanomaterials.[283] Nondestructive PFM modalities will likely come practical alternatives to measure the piezoelectricity in soft nanomaterials.[284]
6) The authors believe that numerous advancements have been introduced into this research area, from establishing PFM to setting additional methods. Till now, we are still trying to specify a single and utterly correct technique to quantify the piezoelectric coefficient of nanomaterials. Although PFM offers a valued platform to characterize the piezoelectricity of nanomaterials, we are still considering it as a regular test-bench tool for industrial applications. To make PFM measurements reliable and consistent, a standardized method is needed. A procedure for best characterization practice ought to be illustrated to identify the vulnerability initiated by potential factors, for example, using tips with various features. For this objective, commercially accessible piezoelectric samples, such as the lithium niobate, could be used to calibrate the PFM setup.

Regardless of such challenges, the field of bioresorbable piezoelectric materials is expanding quickly. Considering the current development in material science and the biomedical engineering field, innovative solutions will assist in overcoming such challenges in the future to alleviate the implementation of biodegradable piezoelectric material in the biomedical engineering field. The latest improvements in the development of biodegradable piezoelectric polymers and manufacturing will continue to introduce efficient treatments in medicine and new diagnostic tools. Bioresorbable piezoelectric polymers hold great potential as an impending group of functional polymers for electromechanical applications. Their intrinsic features place them at the top position for biomedical applications with environmental sustainability, biosafety, and incomparable biocompatibility. Many exciting research opportunities based on biodegradable piezoelectric materials will introduce groundbreaking basic understandings. We expect the natural and synthetic bio-piezoelectric polymers group will soon emerge as a potential interdisciplinary subfield at the junction between biomedical engineering and material science.

Acknowledgements

M.A and L.B. are supported by The Scientific and Technological Research Council of Turkey (TUBITAK) 2232 (funding #118C295), 2244 (#118C155), and 3501 (120M363) programs. L.B. acknowledges the support through a Marie Skłodowska-Curie Individual Fellowship (H2020-MSCA-IF-2018-840786, Brain Watch).

Conflict of Interest

The authors declare no conflict of interest.

Keywords

biodegradables, biomedical devices, piezoelectric polymers

Received: January 30, 2023
Revised: May 21, 2023
Published online: June 9, 2023

[1] H. Cui, R. Hensleigh, D. Yao, D. Maurya, P. Kumar, M. G. Kang, S. Priya, X. R. Zheng, *Nat. Mater.* **2019**, *18*, 234.
[2] M. De Jong, W. Chen, H. Geerlings, M. Asta, K. A. Persson, *Sci. Data* **2015**, *2*, 150053.
[3] B. Malic, T. Rojac, *Nat. Mater.* **2018**, *17*, 297.
[4] M. T. Chorsi, E. J. Curry, H. T. Chorsi, R. Das, J. Baroody, P. K. Purohit, H. Ilies, T. D. Nguyen, *Adv. Mater.* **2019**, *31*, 1802084.
[5] K. S. Ramadan, D. Sameoto, S. Evoy, *Smart Mater. Struct.* **2014**, *23*, 033001.

[6] N. Sezer, M. Koç, *Nano Energy* **2021**, *80*, 105567.
[7] H. Yuan, T. Lei, Y. Qin, R. Yang, *Nano Energy* **2019**, *59*, 84.
[8] F. Jiang, X. Zhou, J. Lv, J. Chen, J. Chen, H. Kongcharoen, Y. Zhang, P. S. Lee, *Adv. Mater.* **2022**, *34*, 2200042.
[9] R. Singh, M. J. Bathaei, E. Istif, L. Beker, *Adv. Healthcare Mater.* **2020**, *9*, 2000790.
[10] V. L. Stuber, D. B. Deutz, J. Bennett, D. Cannel, D. M. de Leeuw, S. van der Zwaag, P. Groen, *Energy Technol.* **2019**, *7*, 177.
[11] F. Rubio-Marcos, J. F. Fernandez, D. A. Ochoa, J. E. García, R. E. Rojas-Hernandez, M. Castro, L. Ramajo, *J. Eur. Ceram. Soc.* **2017**, *37*, 3501.
[12] T. Zheng, J. Wu, D. Xiao, J. Zhu, *Prog. Mater. Sci.* **2018**, *98*, 552.
[13] R. A. Surmenev, R. V Chernozem, I. O. Pariy, M. A. Surmeneva, *Nano Energy* **2021**, *79*, 105442.
[14] F. Liu, N. A. Hashim, Y. Liu, M. R. M. Abed, K. Li, *J. Memb. Sci.* **2011**, *375*, 1.
[15] J. Lu, S. Hu, W. Li, X. Wang, X. Mo, X. Gong, H. Liu, W. Luo, W. Dong, C. Sima, Y. Wang, G. Yang, J. T. Luo, S. Jiang, Z. Shi, G. Zhang, *ACS Nano* **2022**, *16*, 3744.
[16] M. Mohammadkhah, D. Marinkovic, M. Zehn, S. Checa, *Bone* **2019**, *127*, 544.
[17] A. C. Ahn, A. J. Grodzinsky, *Med. Eng. Phys.* **2009**, *31*, 733.
[18] M. Minary-Jolandan, M.-F. Yu, *Nanotechnology* **2009**, *20*, 085706.
[19] J. Sun, H. Guo, J. Ribera, C. Wu, K. Tu, M. Binelli, G. Panzarasa, F. W. M. R. Schwarze, Z. L. Wang, I. Burgert, *ACS Nano* **2020**, *14*, 14665.
[20] Z. Fang, H. Zhang, S. Qiu, Y. Kuang, J. Zhou, Y. Lan, C. Sun, G. Li, S. Gong, Z. Ma, *Adv. Mater. Technol.* **2021**, *6*, 2000928.
[21] J. Sun, H. Guo, G. N. Schädli, K. Tu, S. Schär, F. W. M. R. Schwarze, G. Panzarasa, J. Ribera, I. Burgert, *Sci. Adv.* **2021**, *7*, eabd9138.
[22] E. J. Curry, K. Ke, M. T. Chorsi, K. S. Wrobel, A. N. Miller, A. Patel, I. Kim, J. Feng, L. Yue, Q. Wu, *Proc. Natl. Acad. Sci. USA* **2018**, *115*, 909.
[23] G. Ico, A. Myung, B. S. Kim, N. V. Myung, J. Nam, *Nanoscale* **2018**, *10*, 2894.
[24] Z. L. Wang, J. Song, *Science* **2006**, *312*, 242.
[25] X. Song, F. Hui, K. Gilmore, B. Wang, G. Jing, Z. Fan, E. Grustan-Gutierrez, Y. Shi, L. Lombardi, S. A. Hodge, *Nanoscale* **2017**, *9*, 6237.
[26] Q. Xu, X. Gao, S. Zhao, Y. Liu, D. Zhang, K. Zhou, H. Khanbareh, W. Chen, Y. Zhang, C. Bowen, *Adv. Mater.* **2021**, *33*, 2008452.
[27] P. R. Tulip, S. J. Clark, *Phys. Rev. B* **2006**, *74*, 64301.
[28] P. R. Tulip, S. J. Clark, *J. Chem. Phys.* **2004**, *121*, 5201.
[29] Y. Zhang, Y. Bao, D. Zhang, C. R. Bowen, *J. Am. Ceram. Soc.* **2015**, *98*, 2980.
[30] S. K. Karan, S. Maiti, J. K. Kim, B. B. Khatua, *Sustainable Materials for Next Generation Energy Devices*, Elsevier, Amsterdam **2021**, pp. 251–282.
[31] I. L. Guy, S. Muensit, E. M. Goldys, *Appl. Phys. Lett.* **1999**, *75*, 4133.
[32] R. E. Newnham, *Properties of Materials: Anisotropy, Symmetry, Structure*, Oxford University, Oxford **2005**.
[33] V. S. Bystrov, I. K. Bdikin, A. Heredia, R. C. Pullar, E. D. Mishina, A. S. Sigov, A. L. Kholkin, *Piezoelectric Nanomaterials for Biomedical Applications*, Springer, Berlin **2012**, pp. 187–211.
[34] T. Someya, *Stretchable Electronics*, John Wiley & Sons, Hoboken, NJ **2012**.
[35] G. da Cunha Rodrigues, P. Zelenovskiy, K. Romanyuk, S. Luchkin, Y. Kopelevich, A. Kholkin, *Nat. Commun.* **2015**, *6*, 7572.
[36] S. Vasilev, P. Zelenovskiy, D. Vasileva, A. Nuraeva, V. Y. Shur, A. L. Kholkin, *J. Phys. Chem. Solids* **2016**, *93*, 68.
[37] S. K. Ghosh, D. Mandal, *Nano Energy* **2016**, *28*, 356.
[38] D. Denning, J. I. Kilpatrick, E. Fukada, N. Zhang, S. Habelitz, A. Fertala, M. D. Gilchrist, Y. Zhang, S. A. M. Tofail, B. J. Rodriguez, *ACS Biomater. Sci. Eng.* **2017**, *3*, 929.
[39] J. Wang, C. Carlos, Z. Zhang, J. Li, Y. Long, F. Yang, Y. Dong, X. Qiu, Y. Qian, X. Wang, *ACS Appl. Mater. Interfaces* **2020**, *12*, 26399.
[40] R. L. Horan, K. Antle, A. L. Collette, Y. Wang, J. Huang, J. E. Moreau, V. Volloch, D. L. Kaplan, G. H. Altman, *Biomaterials* **2005**, *26*, 3385.
[41] A. Stapleton, M. R. Noor, J. Sweeney, V. Casey, A. L. Kholkin, C. Silien, A. A. Gandhi, T. Soulimane, S. A. M. Tofail, *Appl. Phys. Lett.* **2017**, *111*, 142902.
[42] X. Dong, M. Ospeck, K. H. Iwasa, *Biophys. J.* **2002**, *82*, 1254.
[43] E. Fukada, *IEEE Trans. Ultrason. Ferroelectr. Freq. Control* **2000**, *47*, 1277.
[44] E. Praveen, S. Murugan, K. Jayakumar, *RSC Adv.* **2017**, *7*, 35490.
[45] N. A. Hoque, P. Thakur, P. Biswas, M. M. Saikh, S. Roy, B. Bagchi, S. Das, P. P. Ray, *J. Mater. Chem. A* **2018**, *6*, 13848.
[46] S. Guerin, A. Stapleton, D. Chovan, R. Mouras, M. Gleeson, C. McKeown, M. R. Noor, C. Silien, F. M. F. Rhen, A. L. Kholkin, *Nat. Mater.* **2018**, *17*, 180.
[47] S. Guerin, J. O'Donnell, E. U. Haq, C. McKeown, C. Silien, F. M. F. Rhen, T. Soulimane, S. A. M. Tofail, D. Thompson, *Phys. Rev. Lett.* **2019**, *122*, 47701.
[48] S. Guerin, T. A. M. Syed, D. Thompson, *Nanoscale* **2018**, *10*, 9653.
[49] S. Guerin, S. A. M. Tofail, D. Thompson, *Cryst. Growth Des.* **2018**, *18*, 4844.
[50] D. Farrar, K. Ren, D. Cheng, S. Kim, W. Moon, W. L. Wilson, J. E. West, S. M. Yu, *Adv. Mater.* **2011**, *23*, 3954.
[51] F. Yang, J. Li, Y. Long, Z. Zhang, L. Wang, J. Sui, Y. Dong, Y. Wang, R. Taylor, D. Ni, *Science* **2021**, *373*, 337.
[52] A. S. Zviagin, R. V Chernozem, M. A. Surmeneva, M. Pyeon, M. Frank, T. Ludwig, P. Tutacz, Y. F. Ivanov, S. Mathur, R. A. Surmenev, *Eur. Polym. J.* **2019**, *117*, 272.
[53] J. Zhang, S. Gong, C. Wang, D. Jeong, Z. L. Wang, K. Ren, *Macromol. Mater. Eng.* **2019**, *304*, 1900259.
[54] B. Y. Lee, J. Zhang, C. Zueger, W.-J. Chung, S. Y. Yoo, E. Wang, J. Meyer, R. Ramesh, S.-W. Lee, *Nat. Nanotechnol.* **2012**, *7*, 351.
[55] S. K. Ghosh, D. Mandal, *Appl. Phys. Lett.* **2017**, *110*, 123701.
[56] E. Fukada, I. Yasuda, *J. Phys. Soc. Japan* **1957**, *12*, 1158.
[57] E. Fukada, S. Sasaki, *J. Polym. Sci., Polym. Phys. Ed.* **1975**, *13*, 1845.
[58] Z. Zhao, Y. Dai, S. X. Dou, J. Liang, *Mater. Today Energy* **2021**, *20*, 100690.
[59] D. Vasilescu, R. Cornillon, G. Mallet, *Nature* **1970**, *225*, 635.
[60] V. V Lemanov, *Ferroelectrics* **2000**, *238*, 211.
[61] V. V Lemanov, S. N. Popov, *Phys. Solid State* **1998**, *40*, 991.
[62] V. V Lemanov, S. N. Popov, G. A. Pankova, *Phys. Solid State* **2002**, *44*, 1929.
[63] V. V Lemanov, S. N. Popov, G. A. Pankova, *Phys. Solid State* **2011**, *53*, 1191.
[64] F. Okosun, S. Guerin, M. Celikin, V. Pakrashi, *Cell Rep.* **2021**, *2*, 100434.
[65] E. S. Hosseini, L. Manjakkal, D. Shakthivel, R. Dahiya, *ACS Appl. Mater. Interfaces* **2020**, *12*, 9008.
[66] A. G. Kordlar, J. Koohsorkhi, E. T. Nejad, *Solid State Electron.* **2021**, *186*, 108168.
[67] L. Qiao, G. Li, H. Tao, J. Wu, Z. Xu, F. Li, *Ceram. Int.* **2020**, *46*, 5641.
[68] A. B. M. Buanz, S. Gaisford, *Cryst. Growth Des.* **2017**, *17*, 1245.
[69] A. V Gerasimov, L. S. Zubaidullina, A. S. Safiullina, R. N. Nagrimanov, M. A. Ziganshin, A. E. Boldyrev, in *AIP Conference Proceedings*, AIP Publishing LLC, College Park, MD **2022**, p. 30020.
[70] M. E. Lines, A. M. Glass, *Principles and Applications of Ferroelectrics and Related Materials*, Oxford University Press, Oxford **2001**.
[71] J. Li, Y. Liu, Y. Zhang, H.-L. Cai, R.-G. Xiong, *Phys. Chem. Chem. Phys.* **2013**, *15*, 20786.
[72] V. S. Bystrov, E. Seyedhosseini, S. Kopyl, I. K. Bdikin, A. L. Kholkin, *J. Appl. Phys.* **2014**, *116*, 066803.
[73] S. Horiuchi, Y. Tokunaga, G. Giovannetti, S. Picozzi, H. Itoh, R. Shimano, R. Kumai, Y. Tokura, *Nature* **2010**, *463*, 789.
[74] V. S. Bystrov, E. Seyedhosseini, I. Bdikin, S. Kopyl, S. M. Neumayer, J. Coutinho, A. L. Kholkin, *Ferroelectrics* **2015**, *475*, 107.

[75] D. Vasileva, S. Vasilev, A. L. Kholkin, V. Y. Shur, *Materials* **2019**, *12*, 1223.
[76] E. Fischer, E. Fischer, E. Fourneau, *Ueber Einige Derivate Des Glykocolls*, Springer, Berlin **1906**.
[77] A. Heredia, V. Meunier, I. K. Bdikin, J. Gracio, N. Balke, S. Jesse, A. Tselev, P. K. Agarwal, B. G. Sumpter, S. V Kalinin, *Adv. Funct. Mater.* **2012**, *22*, 2996.
[78] K. Jenkins, S. Kelly, V. Nguyen, Y. Wu, R. Yang, *Nano Energy* **2018**, *51*, 317.
[79] K. Ryan, J. Beirne, G. Redmond, J. I. Kilpatrick, J. Guyonnet, N.-V. Buchete, A. L. Kholkin, B. J. Rodriguez, *ACS Appl. Mater. Interfaces* **2015**, *7*, 12702.
[80] A. Kholkin, N. Amdursky, I. Bdikin, E. Gazit, G. Rosenman, *ACS Nano* **2010**, *4*, 610.
[81] S. Safaryan, V. Slabov, S. Kopyl, K. Romanyuk, I. Bdikin, S. Vasilev, P. Zelenovskiy, V. Y. Shur, E. A. Uslamin, E. A. Pidko, *ACS Appl. Mater. Interfaces* **2018**, *10*, 10543.
[82] V. Nguyen, K. Jenkins, R. Yang, *Nano Energy* **2015**, *17*, 323.
[83] V. Nguyen, R. Zhu, K. Jenkins, R. Yang, *Nat. Commun.* **2016**, *7*, 13566.
[84] Z. Tao, H. Yuan, S. Ding, Y. Wang, W. Hu, R. Yang, *Nano Energy* **2021**, *88*, 106229.
[85] Y. Kim, H. Park, Y. Kim, C. Lee, H. Park, J.-H. Lee, *ACS Appl. Mater. Interfaces* **2022**, *14*, 38778.
[86] H. Park, Y. Kim, Y. Kim, C. Lee, H. Park, H. Joo, J. H. Lee, J.-H. Lee, *Appl. Surf. Sci.* **2023**, *618*, 156588.
[87] I. Bdikin, V. Bystrov, *Appl. Phys. Lett.* **2012**, *100*, 043702.
[88] A. Handelman, P. Beker, E. Mishina, S. Semin, N. Amdursky, G. Rosenman, *Ferroelectrics* **2012**, *430*, 84.
[89] Z. Gan, X. Wu, X. Zhu, J. Shen, *Angew. Chem., Int. Ed.* **2013**, *52*, 2055.
[90] V. S. Bystrov, E. Paramonova, I. Bdikin, S. Kopyl, A. Heredia, R. C. Pullar, A. L. Kholkin, *Ferroelectrics* **2012**, *440*, 3.
[91] H. R. Leuchtag, *Voltage-Sensitive Ion Channels: Biophysics of Molecular Excitability*, Springer, Berlin **2008**.
[92] H. R. Leuchtag, *Ferroelectrics* **2000**, *236*, 23.
[93] V. S. Bystrov, H. R. Leuchtag, *Ferroelectrics* **1994**, *155*, 19.
[94] A. Chen, C.-D. Poon, T. J. Dingemans, E. T. Samulski, *Liq. Cryst.* **1998**, *24*, 255.
[95] S. Guerin, S. A. M. Tofail, D. Thompson, *NPG Asia Mater.* **2019**, *11*, 10.
[96] W. Gindl, G. Emsenhuber, J. Plackner, J. Konnerth, J. Keckes, *Biomacromolecules* **2010**, *11*, 1281.
[97] K. Kemp, J. Griffiths, S. Campbell, K. Lovell, *J. Crohn's Colitis* **2013**, *7*, e386.
[98] Y. García, Y. B. Ruiz-Blanco, Y. Marrero-Ponce, C. M. Sotomayor-Torres, *Sci. Rep.* **2016**, *6*, 34616.
[99] L. Csoka, I. C. Hoeger, O. J. Rojas, I. Peszlen, J. J. Pawlak, P. N. Peralta, *ACS Macro Lett.* **2012**, *1*, 867.
[100] H. Du, W. Liu, M. Zhang, C. Si, X. Zhang, B. Li, *Carbohydr. Polym.* **2019**, *209*, 130.
[101] F. Liu, M. W. Urban, *Prog. Polym. Sci.* **2010**, *35*, 3.
[102] S. Rajala, M. Vuoriluoto, O. J. Rojas, S. Franssila, S. Tuukkanen, *Proc. of XXI IMEKO World Cong.*, IMEKO XXI World Congress, Prague, Czech Republic **2015**.
[103] D. Zhao, Y. Zhu, W. Cheng, W. Chen, Y. Wu, H. Yu, *Adv. Mater.* **2021**, *33*, 2000619.
[104] Y. Song, Z. Shi, G.-H. Hu, C. Xiong, A. Isogai, Q. Yang, *J. Mater. Chem. A* **2021**, *9*, 1910.
[105] A. Gaur, S. Tiwari, C. Kumar, P. Maiti, **2020**.
[106] S. Maiti, S. Kumar Karan, J. Lee, A. Kumar Mishra, B. Bhusan Khatua, J. Kon Kim, *Nano Energy* **2017**, *42*, 282.
[107] C. Miao, L. Reid, W. Y. Hamad, *Appl. Mater. Today* **2021**, *24*, 101082.
[108] S. Rajala, T. Siponkoski, E. Sarlin, M. Mettanen, M. Vuoriluoto, A. Pammo, J. Juuti, O. J. Rojas, S. Franssila, S. Tuukkanen, *ACS Appl. Mater. Interfaces* **2016**, *8*, 15607.
[109] S. Horiuchi, Y. Tokura, *Nat. Mater.* **2008**, *7*, 357.
[110] A. Amran, F. B. Ahmad, M. H. M. Akmal, A. A. M. Ralib, M. I. Bin Suhaimi, *Mater. Today Commun.* **2021**, *29*, 102919.
[111] K. Kim, M. Ha, B. Choi, S. H. Joo, H. S. Kang, J. H. Park, B. Gu, C. Park, C. Park, J. Kim, *Nano Energy* **2018**, *48*, 275.
[112] S. M. Joseph, S. Krishnamoorthy, R. Paranthaman, J. A. Moses, C. Anandharamakrishnan, *Carbohydr. Polym. Technol. Appl.* **2021**, *2*, 100036.
[113] W. Ji, H. Yuan, B. Xue, S. Guerin, H. Li, L. Zhang, Y. Liu, L. J. W. Shimon, M. Si, Y. Cao, *Angew. Chem.* **2022**, *134*, e202201234.
[114] H. K. No, S. P. Meyers, W. Prinyawiwatkul, Z. Xu, *J. Food Sci.* **2007**, *72*, R87.
[115] A. K. Bharimalla, S. P. Deshmukh, N. Vigneshwaran, P. G. Patil, V. Prasad, *Polym.-Plast. Technol. Eng.* **2017**, *56*, 805.
[116] S. C. M. Fernandes, C. S. R. Freire, A. J. D. Silvestre, C. Pascoal Neto, A. Gandini, L. A. Berglund, L. Salmén, *Carbohydr. Polym.* **2010**, *81*, 394.
[117] M. N. V. R. Kumar, *React. Funct. Polym.* **2000**, *46*, 1.
[118] F. B. Ahmad, M. H. M. Akmal, A. Amran, M. H. Hasni, *IOP Conf. Ser.: Mater. Sci. Eng.* **2020**, *778*, 012034.
[119] A. Safari, V. F. Janas, *Ferroelectrics* **1997**, *196*, 187.
[120] A. Hänninen, S. Rajala, T. Salpavaara, M. Kellomäki, S. Tuukkanen, *Procedia Eng.* **2016**, *168*, 1176.
[121] C. Ma, H. Wang, Y. Chi, Y. Wang, L. Jiang, N. Xu, Q. Wu, Q. Feng, X. Sun, *Appl. Mater. Today* **2021**, *22*, 100902.
[122] D. Kim, S. A. Han, J. H. Kim, J. Lee, S. Kim, S. Lee, *Adv. Mater.* **2020**, *32*, 1906989.
[123] N. More, G. Kapusetti, *Med. Hypotheses* **2017**, *108*, 10.
[124] K. Kapat, Q. T. H. Shubhra, M. Zhou, S. Leeuwenburgh, *Adv. Funct. Mater.* **2020**, *30*, 1909045.
[125] I. Chae, C. K. Jeong, Z. Ounaies, S. H. Kim, *ACS Appl Bio Mater* **2018**, *1*, 936.
[126] S. K. Ghosh, D. Mandal, *ACS Sustainable Chem. Eng.* **2017**, *5*, 8836.
[127] V. Vivekananthan, N. R. Alluri, Y. Purusothaman, A. Chandrasekhar, S. Selvarajan, S. J. Kim, *ACS Appl. Mater. Interfaces* **2018**, *10*, 18650.
[128] Z. Zhou, D. Qian, M. Minary-Jolandan, *ACS Biomater. Sci. Eng.* **2016**, *2*, 929.
[129] M. Nair, Y. Calahorra, S. Kar-Narayan, S. M. Best, R. E. Cameron, *Nanoscale* **2019**, *11*, 15120.
[130] S. Bera, S. Guerin, H. Yuan, J. O'Donnell, N. P. Reynolds, O. Maraba, W. Ji, L. J. W. Shimon, P.-A. Cazade, S. A. M. Tofail, *Nat. Commun.* **2021**, *12*, 2634.
[131] D.-L. Wen, D.-H. Sun, P. Huang, W. Huang, M. Su, Y. Wang, M.-D. Han, B. Kim, J. Brugger, H.-X. Zhang, *Microsyst. Nanoeng.* **2021**, *7*, 35.
[132] L. Pan, F. Wang, Y. Cheng, W. R. Leow, Y.-W. Zhang, M. Wang, P. Cai, B. Ji, D. Li, X. Chen, *Nat. Commun.* **2020**, *11*, 1332.
[133] T. Yucel, P. Cebe, D. L. Kaplan, *Adv. Funct. Mater.* **2011**, *21*, 779.
[134] I. Chiesa, C. De Maria, M. R. Ceccarini, L. Mussolin, R. Coletta, A. Morabito, R. Tonin, M. Calamai, A. Morrone, T. Beccari, *ACS Appl. Mater. Interfaces* **2022**, *14*, 19253.
[135] C.-T. Pan, C.-K. Yen, M.-C. Hsieh, S.-Y. Wang, C.-H. Chien, J. C.-C. Huang, L. Lin, Y.-L. Shiue, S.-W. Kuo, *ACS Appl. Energy Mater.* **2018**, *1*, 5627.
[136] V. Sencadas, C. Garvey, S. Mudie, J. J. K. Kirkensgaard, G. Gouadec, S. Hauser, *Nano Energy* **2019**, *66*, 104106.
[137] I. W. Park, K. W. Kim, Y. Hong, H. J. Yoon, Y. Lee, D. Gwak, K. Heo, *Nanomaterials* **2020**, *10*, 93.
[138] K. Heo, H.-E. Jin, H. Kim, J. H. Lee, E. Wang, S.-W. Lee, *Nano Energy* **2019**, *56*, 716.

[139] D.-M. Shin, H. J. Han, W.-G. Kim, E. Kim, C. Kim, S. W. Hong, H. K. Kim, J.-W. Oh, Y.-H. Hwang, *Energy Environ. Sci.* **2015**, *8*, 3198.
[140] S. J. Lee, A. P. Arun, K. J. Kim, *Mater. Lett.* **2015**, *148*, 58.
[141] A. Farahani, A. Zarei-Hanzaki, H. R. Abedi, L. Tayebi, E. Mostafavi, *J. Funct. Biomater.* **2021**, *12*, 71.
[142] K. Asaka, H. Okuzaki, *Soft Actuators*, Vol. 10, Springer, **2014**, 974.
[143] G. Zhao, B. Huang, J. Zhang, A. Wang, K. Ren, Z. L. Wang, *Macromol. Mater. Eng.* **2017**, *302*, 1600476.
[144] N. B. Gakkai, Ō. B. Gakkai, *Japan. J. Appl. Phys.* **1982**, *21*.
[145] A. Farahani, A. Zarei-Hanzaki, H. R. Abedi, I. Haririan, M. Akrami, Z. Aalipour, L. Tayebi, *J. Mater. Res. Technol.* **2021**, *15*, 6356.
[146] M. Smith, Y. Calahorra, Q. Jing, S. Kar-Narayan, *APL Mater.* **2017**, *5*, 074105.
[147] J. Zhu, L. Jia, R. Huang, *J. Mater. Sci.* **2017**, *28*, 12080.
[148] E. J. Curry, T. T. Le, R. Das, K. Ke, E. M. Santorella, D. Paul, M. T. Chorsi, K. T. M. Tran, J. Baroody, E. R. Borges, *Proc. Natl. Acad. Sci. USA* **2020**, *117*, 214.
[149] P. Wu, P. Chen, C. Xu, Q. Wang, F. Zhang, K. Yang, W. Jiang, J. Feng, Z. Luo, *Nano Energy* **2022**, *102*, 107707.
[150] Y. M. Yousry, V. Wong, R. Ji, Y. Chen, S. Chen, X. Zhang, D. B. K. Lim, L. Shen, K. Yao, *Adv. Funct. Mater.* **2023**, *33*, 2213582.
[151] T. T. Le, E. J. Curry, T. Vinikoor, R. Das, Y. Liu, D. Sheets, K. T. M. Tran, C. J. Hawxhurst, J. F. Stevens, J. N. Hancock, *Adv. Funct. Mater.* **2022**, *32*, 2113040.
[152] E. D. Bosne, A. Heredia, S. Kopyl, D. V Karpinsky, A. G. Pinto, A. L. Kholkin, *Appl. Phys. Lett.* **2013**, *102*, 073504.
[153] I. Bdikin, V. Bystrov, I. Delgadillo, J. Gracio, S. Kopyl, M. Wojtas, E. Mishina, A. Sigov, A. L. Kholkin, *J. Appl. Phys.* **2012**, *111*, 074104.
[154] A. Heredia, I. Bdikin, S. Kopyl, E. Mishina, S. Semin, A. Sigov, K. German, V. Bystrov, J. Gracio, A. L. Kholkin, *J. Phys. D Appl. Phys.* **2010**, *43*, 462001.
[155] Y. Iitaka, *Nature* **1959**, *183*, 390.
[156] P. Hu, S. Hu, Y. Huang, J. R. Reimers, A. M. Rappe, Y. Li, A. Stroppa, W. Ren, *J. Phys. Chem. Lett.* **2019**, *10*, 1319.
[157] D. Isakov, E. de M. Gomes, I. Bdikin, B. Almeida, M. Belsley, M. Costa, V. Rodrigues, A. Heredia, *Cryst. Growth Des.* **2011**, *11*, 4288.
[158] D. Denning, M. V Paukshto, S. Habelitz, B. J. Rodriguez, *J. Biomed. Mater. Res., Part B* **2014**, *102*, 284.
[159] J. Joseph, S. G. Singh, S. R. K. Vanjari, *IEEE Sens. J.* **2017**, *17*, 8306.
[160] C. Wang, K. Xia, Y. Zhang, D. L. Kaplan, *Acc. Chem. Res.* **2019**, *52*, 2916.
[161] L. Meinel, O. Betz, R. Fajardo, S. Hofmann, A. Nazarian, E. Cory, M. Hilbe, J. McCool, R. Langer, G. Vunjak-Novakovic, *Bone* **2006**, *39*, 922.
[162] Y. Yang, F. Ding, J. Wu, W. Hu, W. Liu, J. Liu, X. Gu, *Biomaterials* **2007**, *28*, 5526.
[163] Y. Wang, H.-J. Kim, G. Vunjak-Novakovic, D. L. Kaplan, *Biomaterials* **2006**, *27*, 6064.
[164] J. H. Lee, J. H. Lee, J. Xiao, M. S. Desai, X. Zhang, S. W. Lee, *Nano Lett.* **2019**, *19*, 2661.
[165] A. Sultana, S. K. Ghosh, V. Sencadas, T. Zheng, M. J. Higgins, T. R. Middya, D. Mandal, *J. Mater. Chem. B* **2017**, *5*, 7352.
[166] E. Fukada, *J. Phys. Soc. Jpn* **1955**, *10*, 149.
[167] E. Fukada, *Wood Sci. Technol.* **1968**, *2*, 299.
[168] V. A. Bazhenov, *Piezoelectric Properties of Wood*, Consultants Bureau, **1961**.
[169] R. J. Moon, A. Martini, J. Nairn, J. Simonsen, J. Youngblood, *Chem. Soc. Rev.* **2011**, *40*, 3941.
[170] A. Jardine, S. Sayed, *Curr. Opin. Green Sustainable Chem.* **2016**, *2*, 34.
[171] T. Yoshida, K. Imoto, K. Tahara, K. Naka, Y. Uehara, S. Kataoka, M. Date, E. Fukada, Y. Tajitsu, *Jpn. J. Appl. Phys.* **2010**, *49*, 09MC11.
[172] T. Ochiai, E. Fukada, *Jpn. J. Appl. Phys.* **1998**, *37*, 3374.
[173] W. Wang, Z. Wu, Z. Dai, Y. Yang, J. Wang, G. Wu, *Amino Acids* **2013**, *45*, 463.
[174] L. Reitzer, *American Society for Microbiology* **2005**, https://doi.org/10.1128/ecosalplus.3.4.7.
[175] P. Béguin, J.-P. Aubert, *FEMS Microbiol. Rev.* **1994**, *13*, 25.
[176] G. Helenius, H. Bäckdahl, A. Bodin, U. Nannmark, P. Gatenholm, B. Risberg, *J. Biomed. Mater. Res. Part A An Off. J. Soc. Biomater. Japanese Soc. Biomater. Aust. Soc. Biomater. Korean Soc. Biomater.* **2006**, *76*, 431.
[177] C. H. Haigler, A. R. White, R. M. Brown Jr, K. M. Cooper, *J. Cell Biol.* **1982**, *94*, 64.
[178] S. D. Dimitrijevich, M. Tatarko, R. W. Gracy, G. E. Wise, L. X. Oakford, C. B. Linsky, L. Kamp, *Carbohydr. Res.* **1990**, *198*, 331.
[179] K. Tomihata, Y. Ikada, *Biomaterials* **1997**, *18*, 567.
[180] H. Sashiwa, H. Saimoto, Y. Shigemasa, R. Ogawa, S. Tokura, *Int. J. Biol. Macromol.* **1990**, *12*, 295.
[181] S. H. Pangburn, P. V Trescony, J. Heller, *Biomaterials* **1982**, *3*, 105.
[182] Y. Cao, B. Wang, *Int. J. Mol. Sci.* **2009**, *10*, 1514.
[183] K. Numata, P. Cebe, D. L. Kaplan, *Biomaterials* **2010**, *31*, 2926.
[184] Y. Wang, D. D. Rudym, A. Walsh, L. Abrahamsen, H.-J. Kim, H. S. Kim, C. Kirker-Head, D. L. Kaplan, *Biomaterials* **2008**, *29*, 3415.
[185] N. Minoura, M. Tsukada, M. Nagura, *Biomaterials* **1990**, *11*, 430.
[186] M. Li, M. Ogiso, N. Minoura, *Biomaterials* **2003**, *24*, 357.
[187] G. J. Laurent, *Am. J. Physiol.* **1987**, *252*, C1.
[188] K. A. Alberti, Q. Xu, *Regen Biomater* **2016**, *3*, 1.
[189] L. Tóthová, J. Bábíčková, P. Celec, *Biotechnol. Appl. Biochem.* **2012**, *59*, 490.
[190] M. Walton, N. J. Cotton, *J. Biomater. Appl.* **2007**, *21*, 395.
[191] O. Laitinen, P. Törmälä, R. Taurio, K. Skutnabb, K. Saarelainen, T. Iivonen, S. Vainionpää, *Biomaterials* **1992**, *13*, 1012.
[192] H. Pistner, D. R. Bendi, J. Mühling, J. F. Reuther, *Biomaterials* **1993**, *14*, 291.
[193] R. R. M. Bos, F. B. Rozema, G. Boering, A. J. Nijenhius, A. J. Pennings, A. B. Verwey, P. Nieuwenhuis, H. W. B. Jansen, *Biomaterials* **1991**, *12*, 32.
[194] J. E. Bergsma, W. C. De Bruijn, F. R. Rozema, R. R. M. Bos, G. Boering, *Biomaterials* **1995**, *16*, 25.
[195] C. S. Lovell, J. M. Fitz-Gerald, C. Park, *J. Polym. Sci., Part B: Polym. Phys.* **2011**, *49*, 1555.
[196] T. Furukawa, E. Fukada, *J. Polym. Sci., Polym. Phys. Ed.* **1976**, *14*, 1979.
[197] Y. Ando, E. Fukada, *J. Polym. Sci., Polym. Phys. Ed.* **1984**, *22*, 1821.
[198] J. Huang, M. S. Lisowski, J. Runt, E. S. Hall, R. T. Kean, N. Buehler, J. S. Lin, *Macromolecules* **1998**, *31*, 2593.
[199] M. Smith, C. Lindackers, K. McCarthy, S. Kar-Narayan, *Macromol. Mater. Eng.* **2019**, *304*, 1800607.
[200] J. W. Lee, Y. Takase, B. A. Newman, J. I. Scheinbeim, *J. Polym. Sci., Part B: Polym. Phys.* **1991**, *29*, 279.
[201] S. Ikeda, T. Saito, M. Nonomura, T. Koda, *Ferroelectrics* **1995**, *171*, 329.
[202] S. Liu, Z. Cui, P. Fu, M. Liu, L. Zhang, Z. Li, Q. Zhao, *J. Polym. Sci., Part B: Polym. Phys.* **2014**, *52*, 1094.
[203] M. Smith, S. Kar-Narayan, *Int. Mater. Rev.* **2022**, *67*, 65.
[204] S.-L. Wu, J. I. Scheinbeim, B. A. Newman, *J. Polym. Sci., Part B: Polym. Phys.* **1999**, *37*, 2737.
[205] E. Fukada, *IEEE Trans. Dielectr. Electr. Insul.* **2006**, *13*, 1110.
[206] W. Hoogsteen, A. R. Postema, A. J. Pennings, G. Ten Brinke, P. Zugenmaier, *Macromolecules* **1990**, *23*, 634.
[207] D. Sawai, K. Takahashi, A. Sasashige, T. Kanamoto, S.-H. Hyon, *Macromolecules* **2003**, *36*, 3601.
[208] P.-H. Ducrot, I. Dufour, C. Ayela, *Sci. Rep.* **2016**, *6*, 19426.
[209] E. Fukada, *Biorheology* **1995**, *32*, 593.
[210] J. H. Lee, K. Heo, K. Schulz-Schönhagen, J. H. Lee, M. S. Desai, H. E. Jin, S. W. Lee, *ACS Nano* **2018**, *12*, 8138.

[211] T. Nakiri, K. Imoto, M. Ishizuka, S. Okamoto, M. Date, Y. Uematsu, E. Fukada, Y. Tajitsu, *Jpn J. Appl. Physics, Part 1 Regul. Pap. Short Notes Rev. Pap.* **2004**, *43*, 6769.
[212] Y. Hwang, Y. Je, D. Farrar, J. E. West, S. M. Yu, W. Moon, *Polymer* **2011**, *52*, 2723.
[213] C. Nicolini, *Biosens. Bioelectron.* **1995**, *10*, 105.
[214] A. Zhang, C. M. Lieber, *Chem. Rev.* **2016**, *116*, 215.
[215] H. Yuk, B. Lu, X. Zhao, *Chem. Soc. Rev.* **2019**, *48*, 1642.
[216] J. Koo, M. R. MacEwan, S.-K. Kang, S. M. Won, M. Stephen, P. Gamble, Z. Xie, Y. Yan, Y.-Y. Chen, J. Shin, *Nat. Med.* **2018**, *24*, 1830.
[217] Q. Guo, J. Koo, Z. Xie, R. Avila, X. Yu, X. Ning, H. Zhang, X. Liang, S. B. Kim, Y. Yan, *Adv. Funct. Mater.* **2019**, *29*, 1905451.
[218] T. Someya, Z. Bao, G. G. Malliaras, *Nature* **2016**, *540*, 379.
[219] C. M. Boutry, L. Beker, Y. Kaizawa, C. Vassos, H. Tran, A. C. Hinckley, R. Pfattner, S. Niu, J. Li, J. Claverie, *Nat. Biomed. Eng.* **2019**, *3*, 47.
[220] C. M. Boutry, A. Nguyen, Q. O. Lawal, A. Chortos, S. Rondeau-Gagné, Z. Bao, *Adv. Mater.* **2015**, *27*, 6954.
[221] E. S. Hosseini, L. Manjakkal, D. Shakthivel, R. Dahiya, in *2020 IEEE Int. Conf. on Flexible and Printable Sensors and Systems*, IEEE, Manchester, UK **2020**, pp. 1–4.
[222] Y. Tajitsu, S. Kawai, M. Kanesaki, M. Date, E. Fukada, *Ferroelectrics* **2004**, *304*, 195.
[223] Y. Tajitsu, M. Kanesaki, M. Tsukiji, K. Imoto, M. Date, E. Fukada, *Ferroelectrics* **2005**, *320*, 133.
[224] Y. Tajitsu, *Polym. Adv. Technol.* **2006**, *17*, 907.
[225] J. Joseph, S. G. Singh, S. R. K. Vanjari, *IEEE Electron Device Lett.* **2018**, *39*, 749.
[226] G. de Marzo, V. M. Mastronardi, L. Algieri, F. Vergari, F. Pisano, L. Fachechi, S. Marras, L. Natta, B. Spagnolo, V. Brunetti, *Adv. Electron. Mater.* **2022**, 2200069.
[227] M. Ando, S. Takeshima, Y. Ishiura, K. Ando, O. Onishi, *Jpn. J. Appl. Phys.* **2017**, *56*, 10PG01.
[228] M. Ando, H. Kawamura, H. Kitada, Y. Sekimoto, T. Inoue, Y. Tajitsu, *Jpn. J. Appl. Phys.* **2013**, *52*, 09KD17.
[229] M. Ando, H. Kawamura, H. Kitada, Y. Sekimoto, T. Inoue, Y. Tajitsu, *2013 IEEE Int. Symp. on Applications of Ferroelectrics*, IEEE, Prague, Czech Republic **2013**, pp. 236–239.
[230] S. Moreno, M. Baniasadi, S. Mohammed, I. Mejia, Y. Chen, M. A. Quevedo-Lopez, N. Kumar, S. Dimitrijevich, M. Minary-Jolandan, *Adv. Electron. Mater.* **2015**, *1*, 1500154.
[231] X. Wang, Y. Gu, Z. Xiong, Z. Cui, T. Zhang, *Adv. Mater.* **2014**, *26*, 1336.
[232] B. Li, X. Hu, Q. Zhang, X. Peng, Y. Xiang, *J. Mater. Sci.* **2021**, *56*, 902.
[233] X. Zhang, C. Zhang, Y. Lin, P. Hu, Y. Shen, K. Wang, S. Meng, Y. Chai, X. Dai, X. Liu, *ACS Nano* **2016**, *10*, 7279.
[234] A. Wang, Z. Liu, M. Hu, C. Wang, X. Zhang, B. Shi, Y. Fan, Y. Cui, Z. Li, K. Ren, *Nano Energy*, Elsevier, **2018**, *43*, 63.
[235] A. Bozkurt, G. A. Brook, S. Moellers, F. Lassner, B. Sellhaus, J. Weis, M. Woeltje, J. Tank, C. Beckmann, P. Fuchs, *Tissue Eng.* **2007**, *13*, 2971.
[236] N. J. Vickers, *Curr. Biol.* **2017**, *27*, R713.
[237] C. C. Silva, D. Thomazini, A. G. Pinheiro, N. Aranha, S. D. Figueiro, J. C. Góes, A. S. B. Sombra, *Mater. Sci. Eng. B* **2001**, *86*, 210.
[238] J. Si, Y. Yang, X. Xing, F. Yang, P. Shan, *Polym. Degrad. Stab.* **2019**, *166*, 73.
[239] C. Shi, Y. Zhu, X. Ran, M. Wang, Y. Su, T. Cheng, *J. Surg. Res.* **2006**, *133*, 185.
[240] Y. Chen, M. Ye, L. Song, J. Zhang, Y. Yang, S. Luo, M. Lin, Q. Zhang, S. Li, Y. Zhou, *Appl. Mater. Today* **2020**, *20*, 100756.
[241] C.-H. Yao, C.-Y. Lee, C.-H. Huang, Y.-S. Chen, K.-Y. Chen, *Mater. Sci. Eng. C* **2017**, *79*, 533.
[242] W.-C. Lin, C.-C. Lien, H.-J. Yeh, C.-M. Yu, S.-H. Hsu, *Carbohydr. Polym.* **2013**, *94*, 603.
[243] Y. Ikada, Y. Shikinami, Y. Hara, M. Tagawa, E. Fukada, *J. Biomed. Mater. Res. An Off. J. Soc. Biomater. Japanese Soc. Biomater.* **1996**, *30*, 553.
[244] M. S. Ramasamy, R. Bhaskar, K. B. Narayanan, S. D. Purohit, S. S. Park, A. Manikkavel, B. Kim, S. S. Han, *Mater. Today Commun.* **2022**, *33*, 104659.
[245] N. B. Barroca, A. L. Daniel-da-Silva, P. S. Gomes, M. H. R. Fernandes, S. Lanceros-Méndez, P. Sharma, A. Gruverman, M. H. V. Fernandes, P. M. Vilarinho, *Microsc. Microanal.* **2012**, *18*, 63.
[246] N. Barroca, P. M. Vilarinho, A. L. Daniel-da-Silva, A. Wu, M. H. Fernandes, A. Gruverman, *Appl. Phys. Lett.* **2011**, *98*, 133705.
[247] D. Santos, D. M. Silva, P. S. Gomes, M. H. Fernandes, J. D. Santos, V. Sencadas, *J. Colloid Interface Sci.* **2017**, *504*, 101.
[248] S. N. Gorodzha, A. R. Muslimov, D. S. Syromotina, A. S. Timin, N. Y. Tcvetkov, K. V Lepik, A. V Petrova, M. A. Surmeneva, D. A. Gorin, G. B. Sukhorukov, *Colloids Surf., B* **2017**, *160*, 48.
[249] M. Sadat-Shojai, M.-T. Khorasani, A. Jamshidi, S. Irani, *Mater. Sci. Eng. C* **2013**, *33*, 2776.
[250] Y.-W. Wang, Q. Wu, J. Chen, G.-Q. Chen, *Biomaterials* **2005**, *26*, 899.
[251] M. P. Prabhakaran, J. Venugopal, S. Ramakrishna, *Acta Biomater.* **2009**, *5*, 2884.
[252] A. Sensini, C. Gualandi, A. Zucchelli, L. A. Boyle, A. P. Kao, G. C. Reilly, G. Tozzi, L. Cristofolini, M. L. Focarete, *Sci. Rep.* **2018**, *8*, 17167.
[253] Z. Yin, X. Chen, J. L. Chen, W. L. Shen, T. M. H. Nguyen, L. Gao, H. W. Ouyang, *Biomaterials* **2010**, *31*, 2163.
[254] S. M. Damaraju, Y. Shen, E. Elele, B. Khusid, A. Eshghinejad, J. Li, M. Jaffe, T. L. Arinzeh, *Biomaterials* **2017**, *149*, 51.
[255] E. Reverchon, L. Baldino, S. Cardea, I. De Marco, *Muscles Ligaments Tendons J* **2012**, *2*, 181.
[256] R. Das, E. J. Curry, T. T. Le, G. Awale, Y. Liu, S. Li, J. Contreras, C. Bednarz, J. Millender, X. Xin, *Nano Energy* **2020**, *76*, 105028.
[257] Y. Jing, X. Ma, C. Xu, H. Tian, S. Chen, *Mater. Sci. Eng. C* **2020**, *117*, 111246.
[258] F. Padilla, R. Puts, L. Vico, K. Raum, *Ultrasonics* **2014**, *54*, 1125.
[259] J. Li, L. Kang, Y. Yu, Y. Long, J. J. Jeffery, W. Cai, X. Wang, *Nano Energy* **2018**, *51*, 728.
[260] Y. Long, H. Wei, J. Li, G. Yao, B. Yu, D. Ni, A. L. F. Gibson, X. Lan, Y. Jiang, W. Cai, *ACS Nano* **2018**, *12*, 12533.
[261] J. Li, L. Kang, Y. Long, H. Wei, Y. Yu, Y. Wang, C. A. Ferreira, G. Yao, Z. Zhang, C. Carlos, *ACS Appl. Mater. Interfaces* **2018**, *10*, 42030.
[262] M. Wang, J. Zhang, Y. Tang, J. Li, B. Zhang, E. Liang, Y. Mao, X. Wang, *ACS Nano* **2018**, *12*, 6156.
[263] Y. Long, Y. Yu, X. Yin, J. Li, C. Carlos, X. Du, Y. Jiang, X. Wang, *Nano Energy* **2019**, *57*, 558.
[264] J. M. Donelan, Q. Li, V. Naing, J. A. Hoffer, D. J. Weber, A. D. Kuo, *Science* **2008**, *319*, 807.
[265] S. P. Beeby, R. N. Torah, M. J. Tudor, P. Glynne-Jones, T. O'Donnell, C. R. Saha, S. Roy, *J. Micromech. Microeng.* **2007**, *17*, 1257.
[266] C. R. Saha, T. O'donnell, N. Wang, P. McCloskey, *Sensors Actuators A Phys.* **2008**, *147*, 248.
[267] C. Nakafuku, S. Takehisa, *J. Appl. Polym. Sci.* **2004**, *93*, 2164.
[268] M. Yasuniwa, S. Tsubakihara, Y. Sugimoto, C. Nakafuku, *J. Polym. Sci., Part B: Polym. Phys.* **2004**, *42*, 25.
[269] J. Ryu, S. Y. Lim, C. B. Park, *Adv. Mater.* **2009**, *21*, 1577.
[270] M. Abbas, A. Atiq, R. Xing, X. Yan, *J. Mater. Chem. B* **2021**, *9*, 4444.
[271] J. Xie, W. Liu, P. G. Schultz, *Angew. Chem.* **2007**, *119*, 9399.
[272] E. Gutierrez, P. A. Burdiles, F. Quero, P. Palma, F. Olate-Moya, H. Palza, *ACS Biomater. Sci. Eng.* **2019**, *5*, 6290.
[273] Q. Zhang, V. N. Mochalin, I. Neitzel, I. Y. Knoke, J. Han, C. A. Klug, J. G. Zhou, P. I. Lelkes, Y. Gogotsi, *Biomaterials* **2011**, *32*, 87.
[274] O. Martin, L. Avérous, *Polymer* **2001**, *42*, 6209.

[275] C. A. Grant, D. J. Brockwell, S. E. Radford, N. H. Thomson, *Biophys. J.* **2009**, *97*, 2985.
[276] J. S. Graham, A. N. Vomund, C. L. Phillips, M. Grandbois, *Exp. Cell Res.* **2004**, *299*, 335.
[277] C. M. Kelly, T. Northey, K. Ryan, B. R. Brooks, A. L. Kholkin, B. J. Rodriguez, N.-V. Buchete, *Biophys. Chem.* **2015**, *196*, 16.
[278] N. B. Sopher, Z. R. Abrams, M. Reches, E. Gazit, Y. Hanein, *J. Micromech. Microeng.* **2007**, *17*, 2360.
[279] S. Almohammed, S. O. Oladapo, K. Ryan, A. L. Kholkin, J. H. Rice, B. J. Rodriguez, *RSC Adv.* **2016**, *6*, 41809.
[280] V. Slabov, D. Vasileva, K. Keller, S. Vasilev, P. Zelenovskiy, S. Kopyl, V. Y. Shur, A. Vinogradov, A. L. Kholkin, *Cryst. Growth Des.* **2019**, *19*, 3869.
[281] P. Güthner, K. Dransfeld, *Appl. Phys. Lett.* **1992**, *61*, 1137.
[282] H. Uršič, U. Prah, *Proc. Math. Phys. Eng. Sci.* **2019**, *475*, 20180782.
[283] Y. Calahorra, W. Kim, J. Vukajlovic-Plestina, A. F. i Morral, S. Kar-Narayan, *Nanotechnology* **2020**, *31*, 404003.
[284] Y. Calahorra, M. Smith, A. Datta, H. Benisty, S. Kar-Narayan, *Nanoscale* **2017**, *9*, 19290.

Mohsin Ali is a graduate student of Biomedical Sciences and Engineering Department at Koç University. He received his bachelor's degree in polymer engineering from the University of Engineering and Technology Lahore, Pakistan. During his undergraduate studies, he worked on fabricating and characterizing elastomers and polymer-based nanocomposites. Currently he is working on bioresorbable, piezoelectric, and elastic polymers for medical applications at Bio-Integrated Microdevices Laboratory.

Levent Beker is currently an assistant professor of mechanical engineering at Koç University. He received his Ph.D. in mechanical engineering from University of California, Berkeley (with Professors Liwei Lin and Albert Pisano) as an HHMI International Student Research Fellow. He was as a postdoctoral research fellow in Chemical Engineering at Stanford University (with Professor Zhenan Bao) during 2017–2019. His current research interests include wearable and implantable biosensors, MEMS, and flexible sensors.